THESIS

BOUNDARY LAYER FEATURES OBSERVED DURING NAME 2004

Submitted by

Elizabeth A. Stuckmeyer

Department of Atmospheric Science

In partial fulfillment of the requirements

For the Degree of Master of Science

Colorado State University

Fort Collins, Colorado

Spring 2011

Master's Committee:

Advisor: Steven A. Rutledge

Richard H. Johnson
Jorge A. Ramirez
Tammy M. Weckwerth

ABSTRACT

BOUNDARY LAYER FEATURES OBSERVED DURING NAME 2004

S-Pol radar data from the North American Monsoon Experiment (NAME) are examined to investigate the characteristics of sea breezes that occurred during the North American Monsoon in the late summer of 2004, as well as their role in modulating monsoon convection. Zero degree plan position indicated (PPI) scans were examined to determine the presence of a sea breeze fine line in the S-Pol radar data. Sea breeze fine lines were typically observed over land very near the coast of the Gulf of California (GoC), and usually moved onshore around 1700-1800 UTC (11:00 AM – 12:00 PM local time), and then continued to move slowly inland on the coastal plain. The sea breezes typically moved on land and dissipated before any significant interactions with Sierra Madre Occidental (SMO) convection could occur. Fine lines varied in reflectivity strength, but were typically around 10 to 20 dBZ. Surface winds from the Estación Obispo (ETO) supersite were analyzed to confirm the presence of a shift in wind direction on days in which a fine line had been identified. Typically winds changed from light and variable to consistently out of the west or southwest.

Vertical plots of S-Pol reflectivity were created to examine sea breeze structure in the vertical, but these were not found to be useful as the sea breeze signature was nearly impossible to distinguish from other boundary layer features. Horizontal structure was further investigated using wind profiler relative reflectivity, vertical velocity, and

horizontal winds from the profiler located at ETO. Relative reflectivity and vertical velocity fields revealed a complex boundary layer structure on some days of repeating updrafts and downdrafts. Further examination of S-Pol PPI data revealed that these vertical motions are likely due to the presence of horizontal convective rolls. Profiler horizontal winds revealed that the depth and vertical structure of the sea breezes varied significantly from day to day, but that the height of the sea breeze is around 1 km above the ground. Sea breezes observed during NAME almost never initiated convection on their own. It is hypothesized that a weak thermal contrast between the GoC and the land leads to comparatively weak sea breezes, which don't have enough lift to trigger convection.

ACKNOWLEDGEMENTS

I would like to thank my advisor, Dr. Steven Rutledge, for his guidance and advice during this project. I would also like to thank Dr. Jorge Ramirez, Dr. Richard Johnson, and Dr. Tammy Weckwerth for serving on my graduate committee. Special thanks to Dr. Leslie Hartten, Paul Johnston, and Dr. Christopher Willliams of NOAA for providing and processing much of the NAME wind profiler data. Additional thanks to Dr. Paul Ciesielski for help with NAME surface and sounding data. I would also like to thank members of the Colorado State University Radar Meteorology group, Dr. Tim Lang, Paul Hein, Nick Guy, Dr. Brenda Dolan Cabell and Angela Rowe for valuable suggestions and programming assistance. Lastly, sincere thanks go to my family and friends for supporting me throughout these past few years. Funding for this research was provided by National Science Foundation grant number ATM-0733396.

TABLE OF CONTENTS

LIST OF TABLES

LIST OF FIGURES

CHAPTER 1

Introduction

1.1 Background and Motivation

In the southwest United States and northwest Mexico, a phenomenon called the North American Monsoon (NAM) plays an important role in forcing and organizing the seasonal distribution of precipitation. In this arid to semi-arid region of the world, correctly forecasting precipitation is vital to the livelihood of people that reside there. However, global forecast models have historically performed poorly on warm-season precipitation forecasts in this region. In 2004, the North American Monsoon Experiment (NAME) was implemented to collect data aimed at increasing understanding about the NAM. Since that time, much knowledge has been gained about large scale forcing and precipitation systems of the monsoon. Some of these features will be revisited later in this chapter. However, smaller scale features within the NAM, including boundary layer features such as sea breezes and roll structures remain largely unexplored The intent of this study is to document such features and identify their roles in contributing to NAM rainfall.

1.2 North American Monsoon

The North American Monsoon (NAM) is a seasonal shift of winds which affects northwest Mexico and the southwest United States. This wind shift results from both the land/sea contrast in the area, as well as the mountainous topography. Topographic features of the core NAM region are displayed in Figure 1.1.

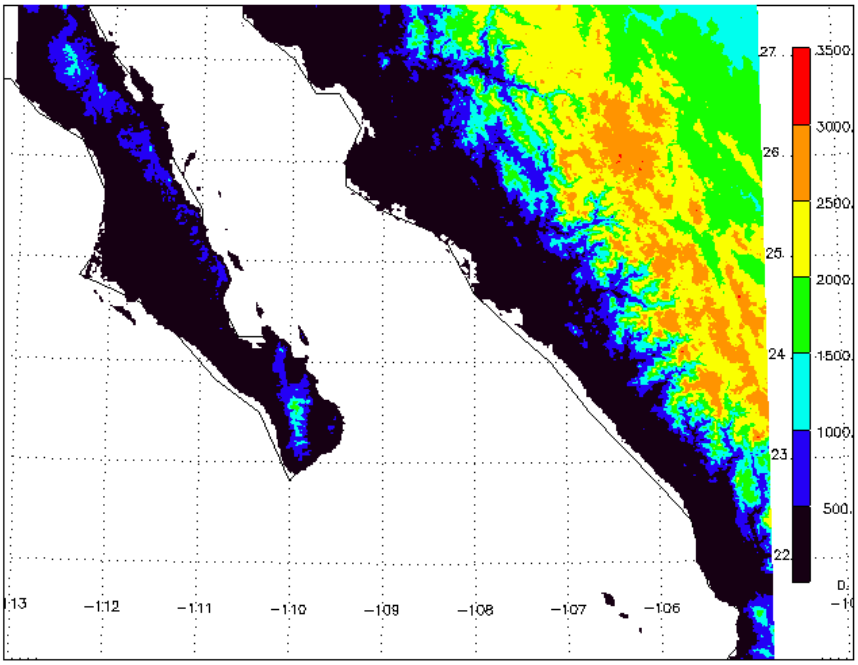

Figure 1.1: Elevation of the core NAM region (meters) in northwestern Mexico. Latitude and longitude (degrees) grids are shown for reference.

Due to the large amount of solar radiation received during the summer months, the land surface warms, creating a thermally driven low pressure center, driving low level air from the ocean to the land. Low-level winds shift from westerly or northwesterly during most of the year to southerly or southeasterly during the monsoon months of July, August, and September.

This shift in mean wind causes a dramatic change in weather patterns, including moisture transport from both the Gulf of Mexico and the Gulf of California (GoC).

Figure 1.2 is a schematic of several dynamic features of the NAM, including low-level jets that supply copious amounts of moisture to northwest Mexico and the southwestern United States, leading to heavy rainfall in that region during the late summer months.

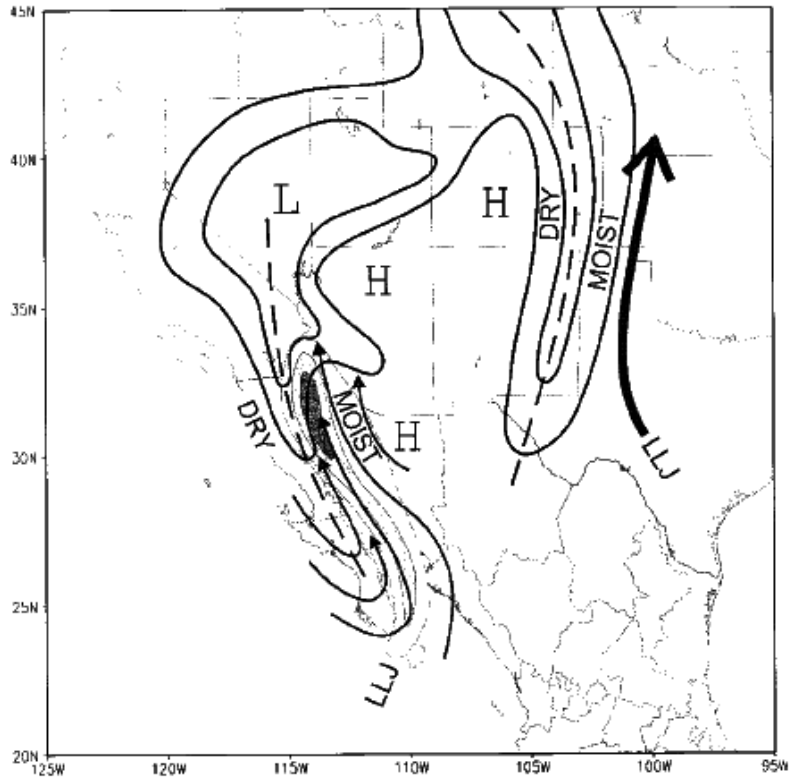

Figure 1.2: Dynamical features of the NAM. Solid dark lines are typical late afternoon 850 mb heights. Thermal lows are marked with an "L". Large arrow indicates the Gulf of Mexico low-level jet. The Gulf of California low-level jet is marked with streamlines and shaded with isotachs (every 2 ms^{-1} starting at 3 ms^{-1}) (From Adams and Comrie 1997, adapted from Douglas 1995).

Additional moisture and the shift in wind direction, combined with elevated topography, leads to the formation of strong diurnally-driven convection. Figure 1.3 shows the percentage of total rainfall in the NAM region that falls during the monsoon months. Greater than 70% of annual precipitation falls during July, August, and September in portions of northwest Mexico.

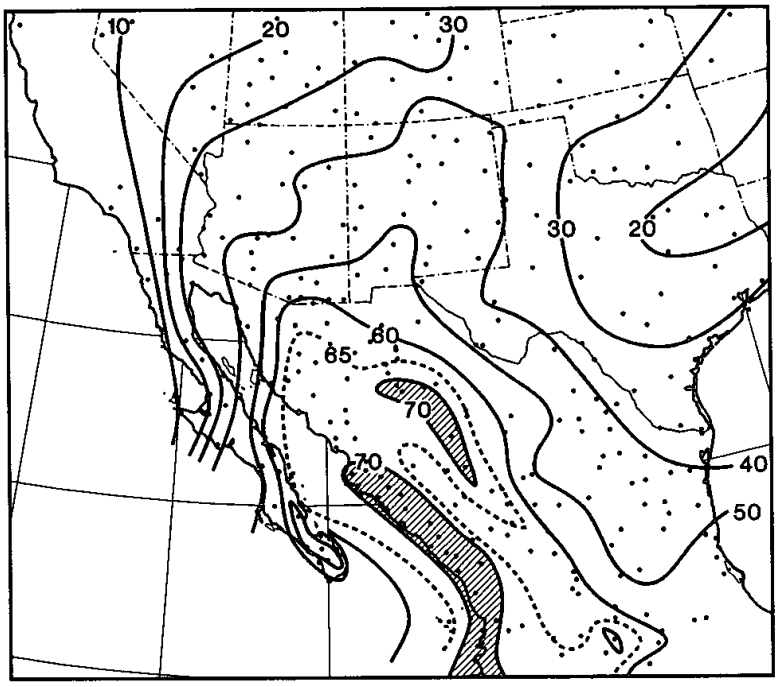

Figure 1.3: Percentage of total annual precipitation in the NAM region that falls during July, August, and September. Areas greater than 70% are crosshatched. Dots indicate surface stations used in the analysis (from Douglas et al. 1993).

In the core NAM region there exist complex interactions between synoptic and mesoscale weather systems, as well as severely varying terrain. Additionally, spatial and temporal variability of the monsoon is not well understood. For this reason, numerical weather prediction (forecast) models have historically performed poorly in forecasting warm-season precipitation in this region and in the adjacent states in the southwest United States (Adams and Comrie 1997). For example, Dunn and Horel (1994) found that convective situations can vary greatly under nearly identical synoptic conditions. To partly address these issues, a field project called the North American Monsoon Experiment was implemented in the summer of 2004.

1.3 NAME Overview

The North American Monsoon Experiment was a field campaign that was conducted during the late summer and early fall of 2004 in Northwest Mexico and the Southwest United States. The aim of this project was to increase understanding of the physical processes and variability of the North American Monsoon, in order to better forecast monsoon precipitation in this region. NAME used a tiered approach to address different scales of processes within the monsoon. The main focus within tier I was to study the structure, organization, and evolution of convective systems, and their interaction with topography. Regional and continental scales were also addressed in tiers II and III, respectively. Figure 1.4 shows the geographical extent of the three tiers used during NAME.

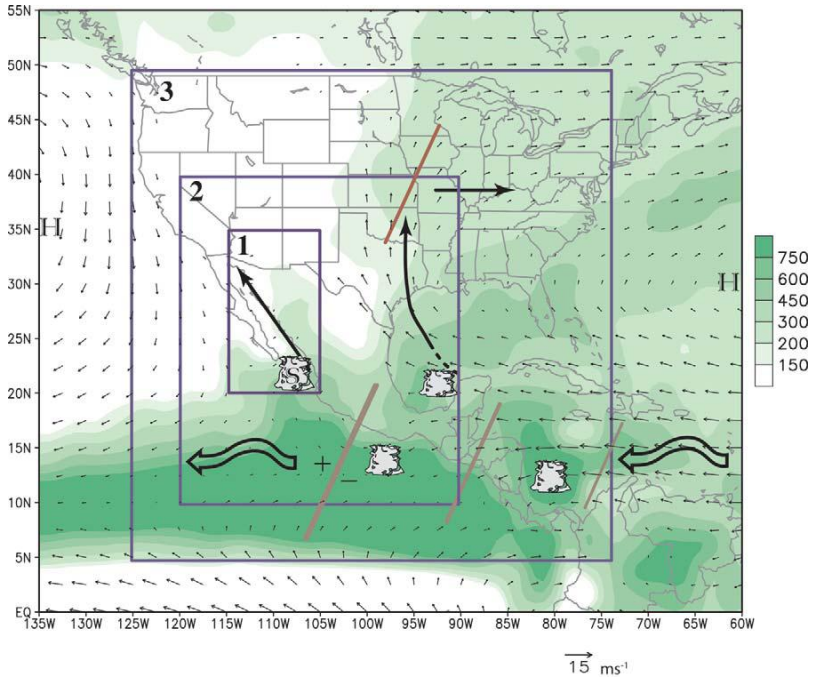

Figure 1.4: Schematic showing the three tiers used during NAME. Green shading shows satellite and rain-gauge combined estimates of precipitation (mm). Also shown are mean 925-hPa vector wind (m/s). The Gulf of California and Great Plains low-level jets are shown with curved and straight arrows, respectively. (From Higgins et al. 2006).

During the project, a large number and variety of field instruments were used to gather data (Higgins et al. 2006). These instruments included surface weather stations, radars, wind profilers, a research ship, radiosondes, rain gauges, instrumented aircraft, and satellite observations. The radar network in particular consisted of three separate radars within tier I, Guasave, Cabo San Lucas, and the NCAR S-Pol radar north of Mazatlán. Figure 1.5 shows the distribution of the NAME radar network.

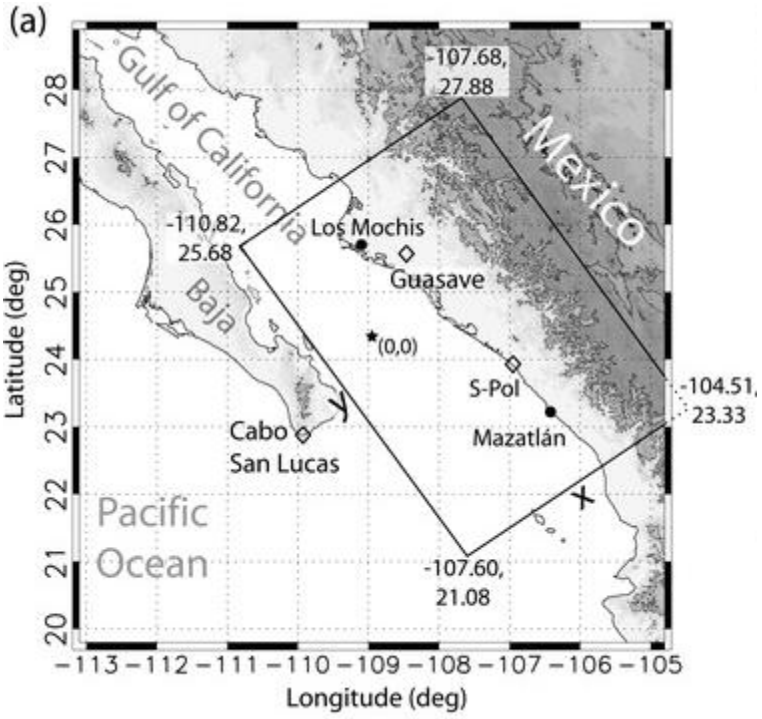

Figure 1.5: NAME radar domain, showing radar locations (diamonds) in relation to some nearby cities. Elevation is shaded.

Scientists from more than 30 different institutions, including universities and government agencies and laboratories, worked on the campaign. These included several different countries, including the United States and Mexico.

1.4 Previous NAME Research

Since NAME was conducted in the summer and fall of 2004, much research has been carried out with the data that was collected. Specifically, the NAME radar network has been used to study the characteristics of precipitation systems and their interactions with topography. The diurnal cycle of convection, as well as vertical characteristics of precipitating storms have also been investigated. The intraseasonal variability of MCS precipitation has also been studied.

1.4.1 Intraseasonal variability of MCS precipitation

Pereira (2008) reported on intraseasonal variability of the North American Monsoon precipitation using the NAME radar network. It was found that of all precipitating features (PFs) observed during NAME 2004, about 95% of these were small short-lived convective cells. Only about 5% of PFs were organized mesoscale convective systems (MCSs). However, these MCSs were responsible for approximately three-quarters of the total precipitation observed in the area sampled by the radar network. The study found that the MCSs varied widely in the amount of precipitation each produced, even in the one season studied. Thermodynamic conditions such as instability and vertical wind shear were found to play a large role in the development and variability of MCSs during NAME.

The role of synoptic conditions in the formation of MCSs with above average rainfall was also examined. Tropical waves were found to be an essential source of instability and moisture, both of which are necessary for MCS development. Pereira (2008) also found that the formation of what was termed the "North American Monsoon

Jet Streak" created favorable large scale rising motion and wind shear profiles under which MCSs were more likely to develop. This jet streak resulted when an upper level inverted trough interacted with an upper level anticyclone.

1.4.2 Diurnal Cycle of NAME Convection

Lang et al. (2007) used the NAME radar network to study the spatial and temporal variability of precipitation in tier I. Overall, the study found that terrain played an important role in the organization of NAM convection. Particularly, terrain features helped to define the diurnal cycle of monsoon precipitation. Typically, convection initialized in the afternoon over the high terrain of the Sierra Madre Occidental (SMO). From there, it tended to grow upscale and traveled westward down the slopes of the SMO toward the coastal plain and the GoC.

Lang et al. (2007) also identified two major regimes of NAM precipitation: regime A and regime B. They found that regime A is characterized by enhanced precipitation over the GoC and coastal plain region. This was especially noticeable during the nighttime and early morning hours. Regime B, on the other hand, was marked by the movement of precipitating storms parallel to the coastline. A third regime, termed AB was defined as periods when both A and B regimes occurred simultaneously. By identifying these different disturbed regimes, Lang et al. (2007) were able to conclude that organized convective systems were responsible for the vast majority of precipitation that fell in the core NAM region.

Rowe et al. (2008) took a more detailed look at the influence of topography on NAME convection. Four elevation groups were defined: over the water, 0-1000 meters

(MSL), 1000-2000 meters, and greater than 2000 meters. Rowe et al. (2008) found that convection was most frequent around 1600 LT over the SMO peaks. Convection at lower elevations was less frequent and typically occurred later in the day, but tended to have higher rain rates than the convection over the SMO.

1.4.3 Vertical Characteristics of NAME Convection

Vertical characteristics of convection as a function of terrain were also investigated using the NAME radar network (Rowe et al. 2008). Generally, convection was found to be shallower over the high terrain, and more vertically developed over the lower elevations. Polarimetric variables were used to investigate the microphysical differences between convection at different topographical elevations. Rowe et al. (2008) found that within areas of high reflectivity, convection over water had smaller median drop diameters and lower differential reflectivity (ZDR) values than did convection that occurred over land. Lang et al. (2010) also found that the drop diameter was smaller in convection over the water, regardless of the observed rain rate. However, Rowe et al. (2008) found little difference in these variables between convection at different elevations over land.

Polarimetric variables also showed that precipitation-sized ice mass was smaller over water than over land. This indicated a basic microphysical difference in land-based monsoon convection compared to convection that occurred over the GoC. From these results, it was hypothesized that convection over the water relies more heavily on warm-rain processes of collision and coalescence than does land-based convection.

Lang et al. (2010) found that the maritime characteristics of smaller drop diameter and reduced ice mass, compared to convection over land, were exaggerated during the disturbed regimes (A, B, and AB mentioned above) identified in Lang et al. 2007. Lang et al. (2010) also found that as elevation decreased over land, drop diameter, precipitation sized ice mass, and liquid water mass all increased. These findings confirm the earlier observations that convection intensifies as it moves off the SMO and into the coastal plain region.

1.4.4 Microphysical Processes in Isolated NAME Convection

Rowe et al. (2011) investigated the microphysical processes that occurred in isolated NAME convection. Specifically, the location, size, and type of hydrometeors in this convection were studied. Various intense convective cells revealed that the polarimetric signatures of NAME convection were comparable to tropical and mid-latitude convection in other areas. These polarimetric data revealed that the presence of ice at high elevations (up to 15 km in one case) indicates that accretional growth processes may play an important role in the production of strong rainfall over high elevations. Additionally, it was found that isolated convection over the high terrain had a narrower drop-size distribution, which suggested that warm-rain processes of collision and coalescence plays a lesser role here than it does in convection over the lower elevations.

1.4.5 Diurnal Cycle of Surface Variables and Air Flow during Name

Zuidema et al. (2007) studied surface variables measured from the ship *Altair* which was located at the mouth of the Gulf of California. Types of variables measured included surface fluxes, atmospheric moisture, and ocean data. The study found that at this location, the mean boundary layer depth was about 410 m. There was also a mean heat flux from the atmosphere into the ocean of 70 W m^{-2}. Radiosonde data revealed a moist layer between 2 and 3 km associated with the land/sea breeze circulation, and another at 5 to 6 km associated with outflow from land-based convection. The diurnal cycle of winds at this location revealed near-surface westerlies associated with the sea breeze. Two different easterly return flows were dominant, at both 2 to 3 km and 5 to 6 km.

Ciesielski and Johnson (2008) examined the variation in surface variables over the entire core region of the monsoon. Using 157 total surface sites, as well as Quick Scatterometer data for ocean winds, an unprecedented dataset was developed. Gridded surface data was produced for the region extending from 15° - 40° N and 90° - 120° W. The data was at a 1 hour temporal resolution and a 0.25° horizontal resolution, and covered the time period from 1 July 2004 – 15 August 2004. Examination of this data revealed what the authors called a "robust" land-sea breeze circulation over most of the GoC. However, they noted that nighttime downslope flow along the SMO was relatively weak, owing to the presence of nocturnal clouds that limited radiational cooling. Soil moisture data revealed that after significant rainfall events, smaller diurnal temperatures and weaker slope flows were observed, due to the presence of increased soil moisture and evapotranspiration.

1.5 Scientific Objectives

This study uses primarily radar and wind profiler data from the North American Monsoon Experiment to address other features of the NAM yet to be studied with the NCAR S-Pol radar dataset, namely boundary layer features consisting of sea breezes and horizontal roll structures. Specific objectives of the study include:

i) To describe in detail the horizontal and vertical structure of the sea breeze front;

ii) To determine the role, or lack thereof, the sea breeze front plays in triggering and organizing daily convection within the NAM region;

iii) To place the sea breeze observed during NAME in context with those observed in other locations, such as Florida;

iv) To describe another prominent boundary layer characteristic observed during NAME, horizontal convective rolls.

Chapter 2 provides a summary of previous research on both sea breezes and horizontal convective rolls. Chapter 3 presents detailed descriptions of all data used in this study, focusing on the S-Pol radar data and the wind profiler data. A description of the methodology, including case selection, is also offered in Chapter 3. Scientific results are detailed in Chapter 4, with subsections on the S-Pol horizontal analysis, vertical structure of the sea breeze front, the sea breeze as a convective trigger, and general boundary layer characteristics. Chapter 5 provides a summary of results from this study.

Chapter 2

Background on Boundary Layer Features

2.1 Sea Breeze Studies

Higgins et al. (2006) has hypothesized that the sea breeze circulation that occurs during the NAM in NW Mexico plays an important role in the modulation of the monsoon convection. Lang et al (2007) suspected that a peak in convection during the afternoon was due to a combination of convection triggered by the sea breeze along the coast and convection originating in the higher terrain. However, prior to this thesis research, an explicit study on the characteristics and behavior of the sea breezes observed during NAME has not been conducted. In order to place this NAME sea breeze study in context, we first review sea breeze studies in other locations.

In many ways, sea breezes are a result of the same basic forcing that causes a monsoon: land and sea thermal contrast. However, sea breeze circulations occur on a much smaller scale than do monsoons. During the day, the land surface warms up faster than the water surface, creating a low-level pressure gradient directed from water to land. This leads to a cool, moist air mass moving onshore, the leading edge of which is referred to as the sea breeze front. In many locations, the sea breeze front has been known to be an important focus for convective intiaition. Both the CaPE field project (Gray 1991) conducted in Florida, and MCTEX (Keenan et al. 2000) in the Tiwi Islands, acknowledged that the daily sea breezes played important roles in triggering diurnal

convection. Knowledge gained by past studies is widespread, however, little is known about the details of sea breezes that occur during the NAM phenomenon.

Sea breezes have been compared to density currents for many years, since a sea breeze is the result of a density difference between two fluids. Simpson (1969;1982) has done much research in this area, comparing laboratory produced density currents to those observed in the atmosphere. Sha et al. (1991) modeled a sea breeze as density current using computer simulations, and is just one of the many studies to do so.

Sea breezes have been studied extensively, even dating back to the 19th century (Davis et al. 1890). Past studies of sea breezes have had a wide range of methodology as well as focus. Early studies of the sea breeze focused on theoretical applications and the development of mathematical equations to explain what was observed (Schmidt 1947; Fisher 1960). Measurement platforms have varied widely and include aircraft, satellite imagery, laboratory simulations, and numerical models.

It has long been acknowledged that weather radar is an effective tool for examining the sea breeze (Donaldson et al. 1953; Atlas et al. 1953; Donaldson 1955; Atlas 1960). Often, the sea breeze front can be detected on radar as a fine line of enhanced reflectivity, even before the development of any convection and resulting precipitation. The strength of the sea breeze is often measured by the strength, in terms of reflectivity value, of the radar observed fine line. Although many research and operational radars are designed to detect precipitation particles in associated storms, clear-air detection is also possible. Precipitation radars can detect scatterers such as insects and perhaps large dust particles (for short wavelength radars in particular) that are caught at the leading edge of the advancing sea breeze front. Weather radars are also

sensitive to changes in the refractive index, as might be present at the leading edge of a sea breeze due to temperature and moisture variations. Long wavelength profilers are particularly useful in documenting the vertical structure of sea breeze fronts as they are sensitive to changes in the index of refraction and clear air returns.

Many previous sea breeze studies have focused on the state of Florida. The Florida peninsula in particular is a prime example of the land/sea thermal contrast required to form land and sea breeze fronts. Nicholls et al. (1991) used a computer model to simulate deep convection over the Florida peninsula. They found that on days lacking any major synoptic scale forcing, the sea breeze determines the location of convection. Furthermore, they found that the convergence of sea breezes from both the east and west coasts of the peninsula can result in development of deep convection.

The Convection and Precipitation/Electrification Experiment (Gray 1991) is one study that resulted in a great deal of research on sea-breeze fronts in Florida. The CaPE experiment was conducted in the summer of 1991. It utilized many different instruments, particularly Doppler radars. Using CaPE data, Atkins and Wakimoto (1997) demonstrated the effect that the synoptic-scale weather patterns can have on sea breeze strength. Sea breezes that occurred in offshore flow regimes were the strongest and widest, in terms of the fine lines observed on radar. On days when the synoptic scale flow was parallel to the shore line, a fine line was only detectable during late afternoon. Lastly, a fine line was not easily visible during onshore flow days. Surface weather stations confirmed these findings, with temperature and moisture gradients strongest on offshore flow days and weakest on onshore flow days.

Another field study that looked at sea breezes in tropical environments was the Maritime Continent Thunderstorm Experiment (MCTEX) (Keenan et al. 2000). This study examined the life cycle of daily convection in the Tiwi Islands in November and December of 1995. Results from this experiment, such as those in Carbone et al. (2000), show that the sea breeze plays an important role in initiating the daily convection. Typically, initial shallow convection forms over the islands in the morning, but as the day goes on, this convection becomes focused along the sea breeze front. As sea breeze convection deepens, it becomes organized on the mesoscale and often forms a convective line. The sea breezes that occur on the Tiwi Islands have some similarity to those that occur on the peninsula of Florida. Since they are islands, it was thought prior to MCTEX that sea breezes from different sides of the island could form and converge in the middle of the island, leading to enhanced convection. However, results have since shown that the sea breezes, while important individually for initiating diurnal convection, did not often collide (Carbone et al. 2000). The sea breezes typically moved too slowly, and significant convection had already formed before a sea breeze merger could occur and have any meaningful strengthening effect.

2.2 Horizontal Convective Rolls

Horizontal convective rolls are one of the most common boundary layer features observed. They occur in the convective boundary layer, and the circulation often appears as lines of cumulus clouds or "cloud streets" where horizontal convergence forces rising motion. They are known, in some cases, to play a role in convective initiation or enhancement of existing convection. Christian and Wakimoto (1989) examined HCRs

that occurred in northeast Colorado. They found that the rolls formed in a well defined boundary layer, and that cloud streets often appeared above, in a stable layer. Radar fine lines were observed underneath the cloud streets. Low level radar echoes were determined to be due to small particulate matter being caught in the updraft portion of the HCR. Echoes at cloud street level above, however, were attributed to refractive index variations (Bragg scatter) at the top of the HCR circulation.

Wilson et al. (1994) and Russell and Wilson (1996) examined the ability of a weather radar to detect horizontal convective rolls in the clear-air boundary layer. They found that the primary scattering mechanism for the boundary layer is Rayleigh scattering off insects, when the temperature is greater than 10° C. They also concluded that the insects are passive tracers, and can therefore be used to reveal air motions within the boundary layer. Additionally it was noted that the updrafts of horizontal convective rolls were observed as thin lines of enhanced reflectivity on the radar display.

Previous studies have shown that the formation of HCRs requires both vertical wind shear and instability. Weckwerth et al. (1999) conducted one of the first studies able to document the entire life cycle of HCRs. In addition to Illinois and Kansas, a major component of the study was data from Florida. One of the major forms of data collection was from the 3 cm X-band component of the dual-frequency CP-2 radar. Often, the first form of boundary layer convection observed in the radar data was horizontal convective rolls. Like in other HCR studies, they found that the roll orientation was determined by the boundary layer wind direction. That is, the rolls aligned themselves with the long axis parallel to the mean wind direction. Unlike previous studies, however, Weckwerth et al. found that the rolls developed even in

boundary layers with relatively insignificant amounts of wind speed and/or shear. Part of this thesis research will document roll structures observed by S-Pol during NAME.

2.3 Interaction between HCRs and Sea Breeze Fronts

Interactions between boundary layer features have been shown to have significant effects on convection. Wakimoto and Atkins (1994) used satellite data, cloud photographs, and radar data from CaPE to examine the relationship between sea breeze fronts and HCRs in Florida. The study found that HCRs served to organize the horizontal structure along the front of the sea breeze. Near-perpendicular intersections of HCRs with the sea breeze front seemed to be preferred location for the development of clouds.

Atkins et al. (1995) continued the study of HCRs and sea breezes. The study used dual-Doppler analysis on the CaPE dataset to identify both sea breeze fronts and horizontal convective rolls (HCRs), as well as study the interaction between the two different boundary layer features. The study showed that often during off-shore flow regimes, when HCRs and sea breeze fronts intersected, the sea breeze front tilted the HCR into the vertical. This interaction led to a deeper updraft and enhanced convection. Figure 2.1 shows a schematic of such an interaction between HCRs and a sea breeze front.

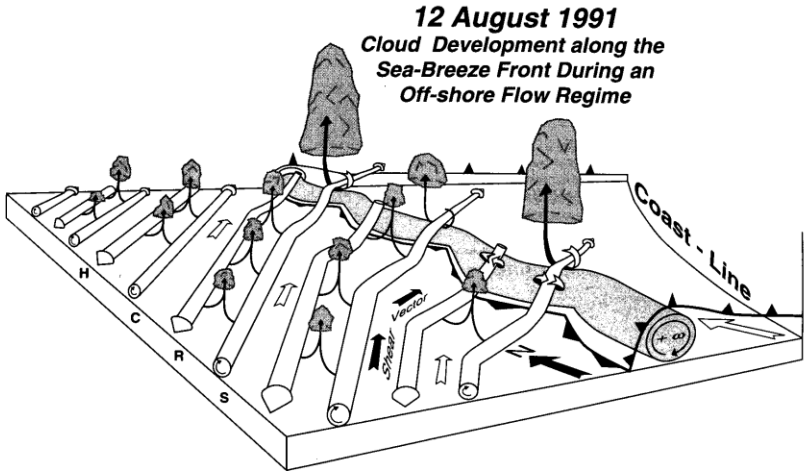

Figure 2.1: Schematic of the interaction between a sea breeze front and horizontal convective rolls during CaPE. The heavy barbed line denotes the sea breeze front, with the circulation lightly shaded. HCRs are shown, unshaded. Horizontal vorticity vectors associated with the roll circulations are shown as white arrows. Clouds are shaded dark gray. The shear vector (solid) and low level winds (unshaded) are also shown. (From Atkins et al. 1995).

The Weckwerth et al. study also investigated the behavior of HCRs in the presence of sea breezes in Florida. It was observed that, as the sea breeze moved inland through the convective boundary layer, the convective features took on the appearance of unorganized cells, rather than well-defined rolls. If winds were light, rolls evolved into open cells. If winds were strong, rolls evolved into unorganized convective elements. Figure 2.2 shows a sample case from this study. The time series of radar reflectivity reveals the boundary layer convection first appearing as rolls (boxes c and d), and then becoming more disorganized as the sea breeze front moves into the field of view (e).

The interaction between sea breeze fronts and HCRs was investigated by Dailey and Fovell (1999). However, rather than using observational data, this study used a computer model to simulate the interaction. The model created an offshore flow regime in which a sharply defined sea breeze front developed. HCRs were also present, and

aligned perpendicular to the sea breeze front. Results from the simulation showed that where the updraft portions of the HCR circulation intersected the sea breeze front, convection was enhanced. Conversely, convection was suppressed where the downdraft branch of the HCR intersected the sea breeze front. The authors noted that the inhibition of convection was particularly evident. This study confirms what others have found: that HCRs can have an effect on the strength of sea breeze convection. With this background, we now turn to a study of sea breeze fronts and HCRs in the NAME 2004 dataset, and to identify their possible roles in triggering or modulating convection.

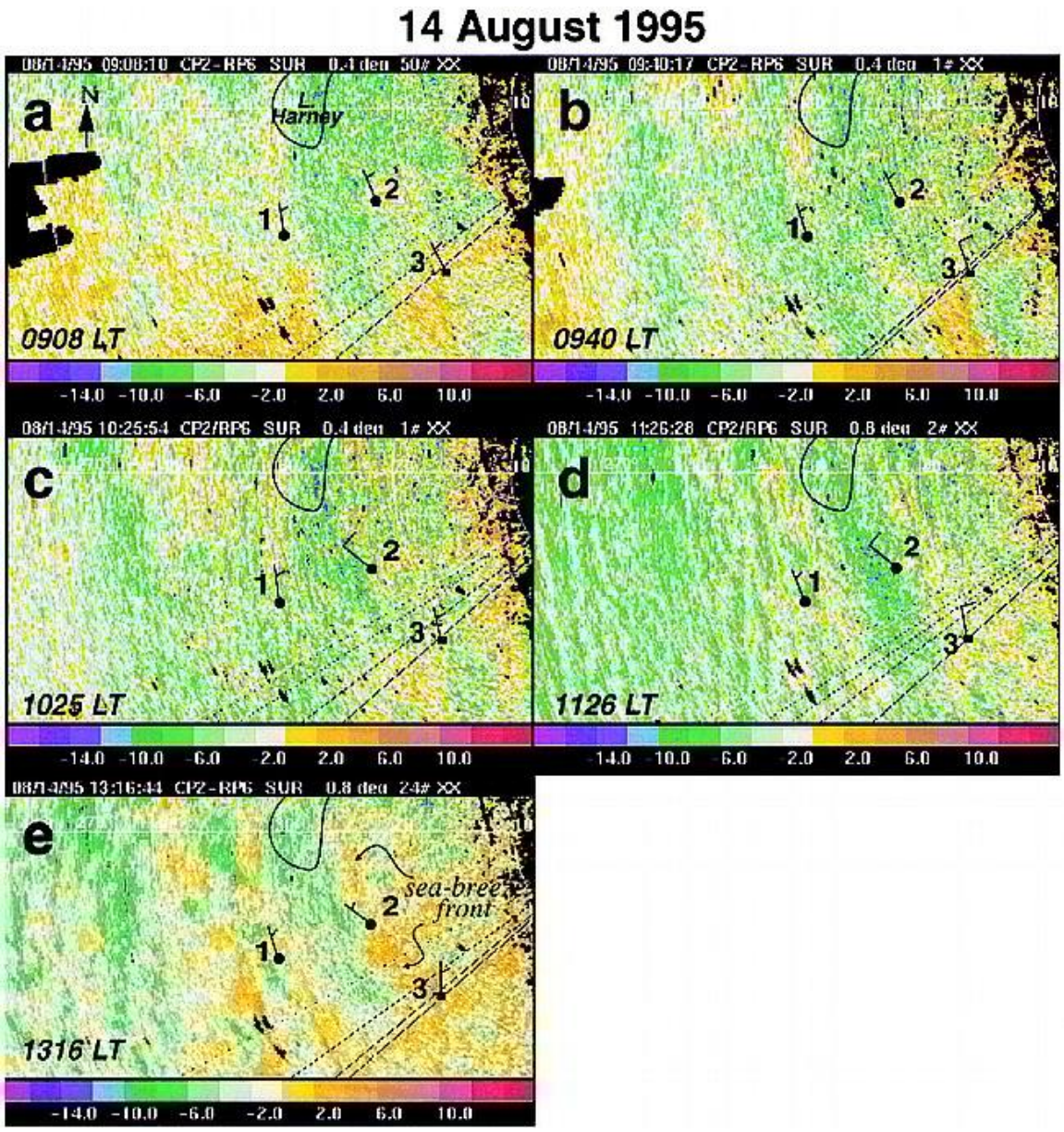

Figure 2.2: Time series of CP-2 X-band radar reflectivity on 14 August 1995. (a) 0908 LT at 0.4 degrees elevation, (b) 0940 LT at 0.4 degrees, (c) 1025 LT at 0.4 degrees, (d) 1126 LT at 0.8 degrees, and (e) 1316 LT at 0.8 degrees. Winds from surface stations are also shown, with a full barb indicating 5 ms^{-1}. In (e) the sea breeze front is marked. (From Weckwerth et al. 1999)

CHAPTER 3

Data and Methodology

3.1 Radar

The radar data used in this study was obtained by the National Center for Atmospheric Research's (NCAR) S-band polarimetric Doppler radar (S-Pol). Figure 3.1 shows the location of S-Pol: about 100 km north of Mazatlán, Mexico at (23.929°N, 106.9521°W), west of the Sierra Madre Occidental (SMO) mountains. S-Pol was operated in NAME from 8 July to 24 August 2004. Two main pulse repetition frequencies (PRFs) of 720 Hz and 960 Hz were used by the radar, with a beamwidth of 1°. The use of these two PRFs resulted in maximum unambiguous ranges of about 210 km and 150 km, respectively.

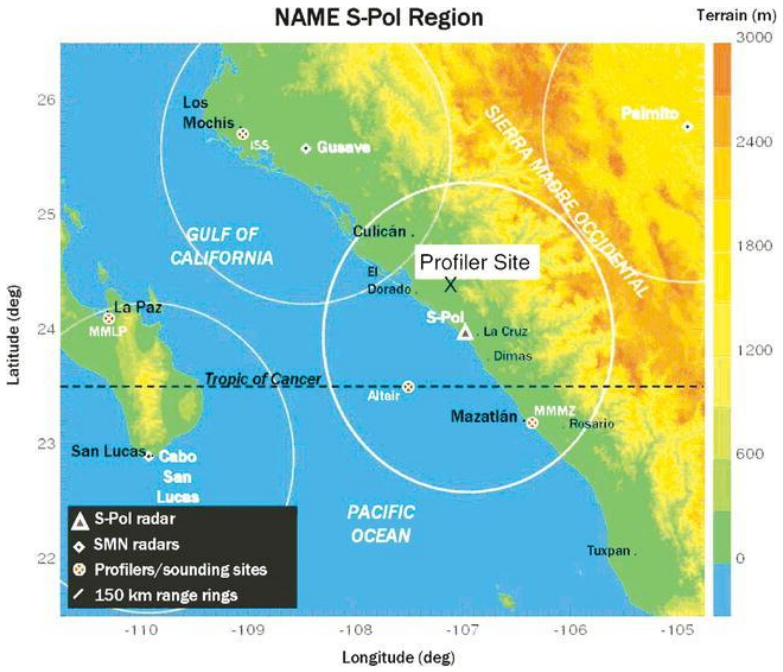

Figure 3.1: Map showing loction of S-Pol and wind profiler in relation to cities in NW Mexico in the core NAM region. The circles indicate 150-km range rings around the radars. Sounding sites used in this study are indicated with red Xs (Altair and MMMZ). (From Williams et al., 2007).

S-Pol utilized several different scanning modes in order to study different aspects of NAME clear-air features and convection. One mode scanned 360° in azimuth to obtain a larger, mesoscale view of storm organization. This mode also focused on low-level scans (elevation angles of 0.8°, 1.3° and 1.8°) to produce rainfall maps using various polarimetric variables out to a range of about 210 km. Two operational weather radars from the Mexican National Weather Service (SMN) radars were also employed during NAME. Data from these radars were combined with the low-mode S-Pol data to improve rainfall mapping abilities. However, data from these two radars was not analyzed for this study.

The second S-Pol mode was a 360° set of plan-position indicator (PPI) scans with higher elevation angles, aimed at studying the vertical structure of precipitation. This

mode also included a 0° scan, specifically designed to sample low-level sea breezes. The 0° scan was investigated in this thesis research. There were also some sector scans done, with a maximum range of about 150 km, as well as a few RHI scans. Both the sector and RHI scans were aimed at studying individual storm evolution and structure.

S-band radars like S-Pol are designed to detect precipitation through Rayleigh scattering of electromagnetic radiation by hydrometeors and biological targets, mainly insects. A component of this study is also to understand the nature of scattering near and around sea breeze fronts where gradients in the index of refraction caused by changes in moisture at the leading edge of sea breezes may provide a component of S-band backscatter. One aim of this study was to determine what scattering mechanisms produced the returns in the S-Pol data pertaining to sea breeze passages.

For this research, raw, unfiltered radar data from S-Pol was used. Typically, studies focusing on precipitation echoes in radar data would filter out clear air signatures such as bugs and boundary lines. Since sea breezes are clear air features, filtering the data could remove some of the sea breeze signature. It should be noted, however, that the unfiltered data contained noise and features such as ground clutter

For the analysis of the S-Pol data, the reflectivity, radial velocity, and differential reflectivity fields were used. These variables were examined in both the horizontal and vertical to gain an understanding of the overall structure of the sea breezes.

3.1.1 PPI Analysis

In order to determine whether or not a sea breeze was present on a particular day, PPI analysis of reflectivity and radial velocity was carried out on the S-Pol data. Visual

analysis of these fields first determined on which days a sea breeze front was detected. First, 0.0° scans were examined for the presence of a fine line of enhanced reflectivity from early morning through mid-day. A fine line due to a sea breeze front would appear as an enhanced line of reflectivity, oriented parallel to the coastline, and moving inland. If such a line was found, the day was considered to have a sea breeze. These cases were later compared with surface wind data for confirmation of a sea breeze passage. PPI animations of cases discussed are available online at: http://radarmet.atmos.colostate.edu/~beth.

3.1.2 RHI Analysis

Range-Height Indicator plots of radar data can be useful for understanding the vertical structure of atmospheric phenomena. While a number of RHI scans were taken by S-Pol during NAME, these were determined by the radar operators on a day-to-day basis, and almost always were done through areas of significant convection. No RHIs were taken through any of the sea breeze fronts. In order to study the vertical structure of the sea breeze fronts, RHIs were reconstructed from individual S-Pol volume scans by gridding the data and interpolating from multiple elevation angles along a single azimuth to form a vertical "slice" of reflectivity. Reconstructed RHIs of reflectivity, radial velocity, and differential reflectivity (ZDR) were created for each of the sea breeze cases.

3.2 Wind Profiler

The wind profiler data used in this study was obtained from a 915 MHz profiler situated about 45 km NNW of the S-Pol radar at (24.28°N, 107.16°W). Figure 3.1 shows

the position of the profiler relative to S-Pol and the city of Mazatlán. This profiler was located near the city of Estación Obispo and is referred to as ETO hereafter.

Wind profilers can be equated to vertically-pointing radars. The profiler used in this study was designed to detect air motions in the lower portions of the atmosphere. Like S-Pol, its data fields included reflectivity (Rayleigh backscatter) and velocity. ETO is also sensitive to changes in the index of refraction (Bragg scatter) and therefore is useful in detecting clear air horizontal and vertical motions.

3.2.1 Relative Reflectivity and Vertical Velocity

Profiler data was quality controlled by removing bad data and points with low signal-to-noise ratios. Time-height plots of uncalibrated reflectivity, hereafter "relative reflectivity," and vertical velocity over ETO were created for each sea breeze case. These plots were used to determine presence and time of sea breeze front passage over the ETO location. The reflectivity was uncalibrated, but was still useful for recognizing any reflectivity enhancements that might be present at the leading edge of the sea breeze. Vertical velocity would be expected to be positive during sea breeze front passage, as the denser air of the sea breeze pushed the less dense air ahead of it and upwards. Similarly, there would be downward motion as a response just after sea breeze passage.

3.2.2 Horizontal Winds

The profiler used in this study was made up of three separate antenna beams, which, when combined, can be used to determine the horizontal air motions directly above the profiler site. Horizontal winds were obtained from the ETO profiler data in

order to gain understanding about the vertical structure of air motions within the sea breeze front. Time-height plots of horizontal wind barbs were created for days with sea breezes as first indicated by S-Pol analysis.

3.3 Upper Air Soundings

Upper air soundings were obtained from two sites in the NAME sounding network (Figure 3.1). Soundings were taken from Mazatlan and the Mexican research ship Altair (location shown in Figure 3.1). These two soundings were used in part to compare the thermal contrast between the land and the ocean in support of the sea breeze component of this study. Refractivity was also calculated using the sounding data. Gradients in the index of refraction can lead to Bragg scattering and resultant radar reflectivity. Thus, the ability to calculate refractivity can be used to evaluate the scattering mechanisms of the sea breeze portion of radar reflectivity. Refractivity (N) can be calculated follows, where T is temperature in Kelvin, p is pressure in millibars, and e is vapor pressure in millibars (Battan 1959):

$$N = \frac{77.6}{T}(p + \frac{4{,}810e}{T})$$

3.4 Surface Data

Surface meteorological measurements were obtained from the same location as the wind profiler data. The Estación Obispo surface station had a two minute time resolution, with data available from 13 July 2004 through 6 January 2005. Time series of surface wind direction and speed were used to confirm the presence of a sea breeze front

passage. A significant wind speed increase and a shift in direction to indicate winds out of the West or Southwest were considered consistent with a sea breeze passage. These wind data were compared to the S-Pol PPI analysis described above. If the change in wind direction did not coincide with the time of fine line appearance on radar, the case was not used, since the sea breeze passage time could not be determined definitively.

3.5 Case Selection and Analysis

Sea breezes were observed on most of the days during NAME. Since they were so prevalent, it was not feasible to present results from every single sea breeze case that was observed. In Chapter 4, analysis will be presented for several cases that exemplify the general characteristics of sea breezes during NAME. The goal of this study is to describe the spectrum of sea breezes observed during the field experiment, their structures, and their possible role in contributing to NAME convection.

CHAPTER 4

Characteristics of Boundary Layer Features

4.1 Introduction

With the previously discussed information about sea breezes and general boundary layer features in tropical locations, discussion of the NAME study results are presented in this chapter. Focus will be on examining a few representative cases from the NAME period. Overall, the role of the sea breeze within the NAME phenomenon will be examined and addressed.

4.2 PPI Analysis

Visual analysis of S-Pol data was initially carried out to look for evidence of sea breeze fronts (SBFs). PPI scans were examined during morning to mid-day hours, the time period during which the sea breeze front would be anticipated to come onshore. The 0-degree elevation angle was the primary scan examined, since it was specifically designed to capture the sea-breeze front. When examining the PPI scans, the features associated with a sea breeze front included a fine line of enhanced reflectivity, relative to the background reflectivity. Additionally, for the fine line to be considered a sea breeze front, it had to be moving inland from the coast of the Gulf of California, and be relatively parallel to the coastline.

Cases were examined using the S-Pol PPI scans from 8 July through 20 August, with data from the first three days considered unusable due to scan testing and working out bugs in the radar operation. Elimination of 8 July, 9 July, and 10 July left 41 potential days with sea breezes to be examined. Sea breeze front characteristics were observed on most of these days, though reflectivity intensity and speed of the fine lines varied widely.

Typically, the fine line was first observed just inland of the S-Pol location, which was very near the coast. Fine-lines associated with sea breeze fronts were not typically observed over the Gulf of California. It is believed that there were not enough clear air scatterers (insects) present over the ocean to support appearance of a sea breeze fine line on radar. Or, due to Earth's curvature, offshore the radar beam heights were above the shallow sea breeze front. However, on a few days, fine lines were observed over the water, but those were determined to be remnants of land breezes that had moved offshore overnight, carrying insects with them. Reflectivites of the fine lines were typically around 10 to 25 dBZ, but varied from case to case. These fine lines were embedded in background reflectivity of around 5 to 10 dBZ. Weaker sea breezes were often hard to distinguish from the background clear-air reflectivity. However, a few of the stronger sea breezes had fine lines that were continuous and could be easily recognized.

Timing of the sea breeze fronts' arrival varied from day-to-day as well. Most commonly, the SBF was first visible on radar by 1700-1800 UTC, or 11:00 AM to noon local time. Occasionally the sea-breeze front was later than normal to arrive, even first showing up on the radar data as late as 2200 UTC (1600 local time). It is speculated that early morning cloud cover over the core NAME region caused a delay in the sea breeze

front's arrival on land, due to decreased solar radiation reaching the land surface, which would reduce the land-sea thermal contrast. PPI scans from a sample of these cases will be discussed in the remainder of this section.

Figure 4.1 shows PPI images from 30 July 2004 from 1743 UTC through 1813 UTC. This day had a typical sea breeze fine line, in that it could be distinguished from the background reflectivity, but was not well defined. The sea breeze front is first visible around 1743 UTC as a weak line oriented NW to SE (denoted with white oval) and just inland of S-Pol (located at 0,0 in the figure). As time progresses, the line becomes more evident on radar and moves inland. Note that ground clutter appears in these images as stationary areas of relatively high reflectivity, such as the region located 15 km east and 20 km north of S-Pol with reflectivity values as high as 45 dBZ. The area near S-Pol, situated NW to SE from about (-9,8) to (10,-10) with reflectivities from about 15 to 30 dBZ is also ground clutter associated with the coast line, and should not be confused with the sea breeze fine line. This clutter is a result of using the raw, unfiltered radar data which was necessary to offer the best detection of the sea breeze front. (An animated loop of this case, as well as others discussed in this chapter, is available online at http://radarmet.atmos.colostate.edu/~beth).

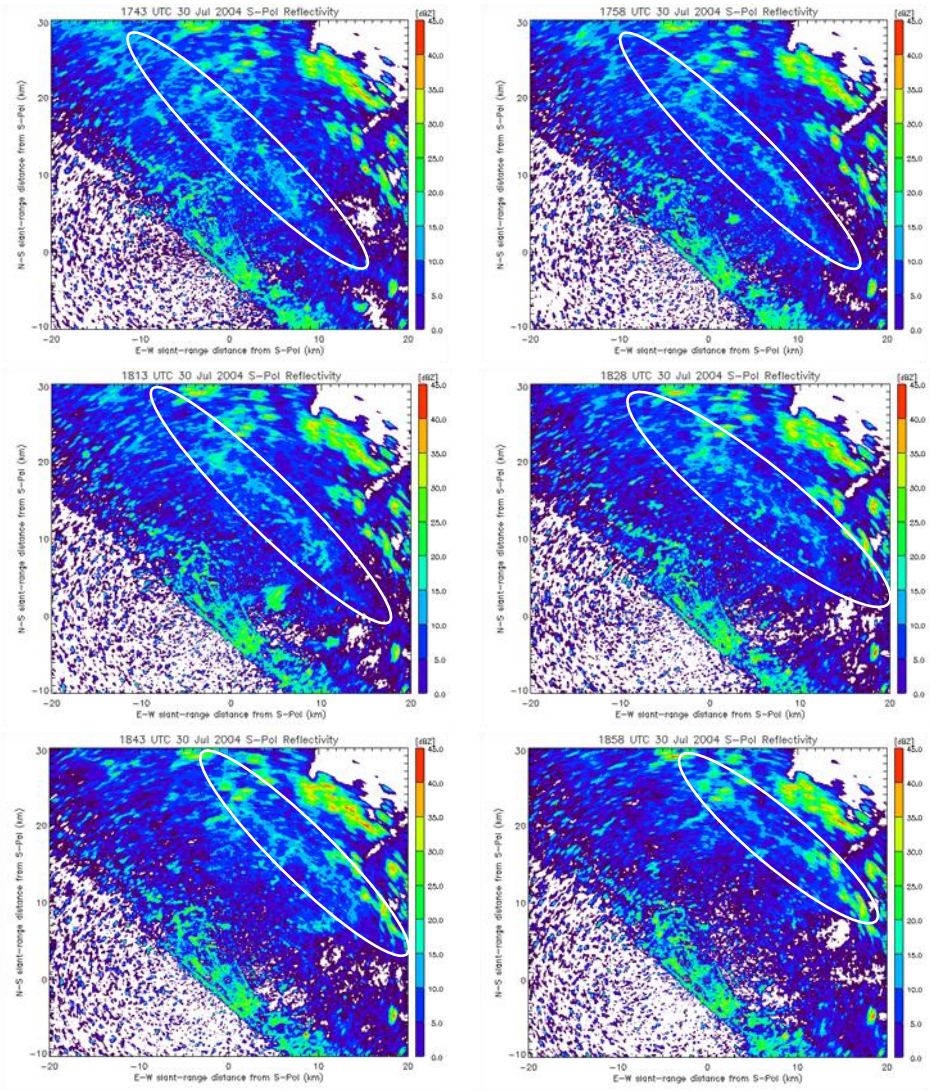

Figure 4.1: S-Pol PPI reflectivity images of 30 July 2004. All scans shown are at an elevation angle of 0.0°. Axes are displayed as slant-range distance (km) from S-Pol, which is located at (0,0). Times (UTC) are displayed at the top of each image. White ovals in each frame indicate the sea breeze fine line.

One of the strongest observed sea breezes, in terms of reflectivity, occurred on 7 August 2004. S-Pol data from this day is shown in Figure 4.2. On this day, the fine line associated with the sea breeze front was relatively wide, and had continuous reflectivities

of 20 to 30 dBZ, making it easy to distinguish. The sea breeze fine line is again marked in Figure 4.2 with ovals. The same areas of ground clutter previously observed in Figure 4.1 are also present. In the times shown in Figure 4.2 (1858 UTC – 2028 UTC), the sea breeze moved about 5 km, or at a speed of roughly 0.93 m/s. Even as one of the stronger sea breezes observed during NAME, it moved relatively slowly.

To show that reflectivity values of this magnitude are realistic for clear air returns, a quick calculation can be carried out using:

$$Z = ND^6 \qquad [4.1]$$

Where Z is reflectivity in mm^6m^{-3}, N is the concentration of particles in m^{-3}, and D is mean diameter of the particles in mm. Considering that for sea breezes, the radar is observing mainly clear-air scattering, it is likely that insects are the primary scattering mechanism (later in the chapter we will discuss index of refraction, or Bragg scattering, as a possible mechanism for sea breeze detection). The size of insects observed by radar varies, and different sources in the literature commonly ranged from 1 mm up to 55 mm in diameter (Hajovsky and LaGrone 1965; Browning and Atlas 1966; Mueller and Larkin 1985). Even with a small insect of 3 mm in diameter, by the above equation it would only take a concentration of about 0.5 m^{-3} to result in an observed reflectivity of 25 dBZ. Larger insects would produce the same reflectivity with even lower concentrations. Thus it can be concluded that reflectivity values of 20 to 30 dBZ in the sea breeze front fine line are reasonable.

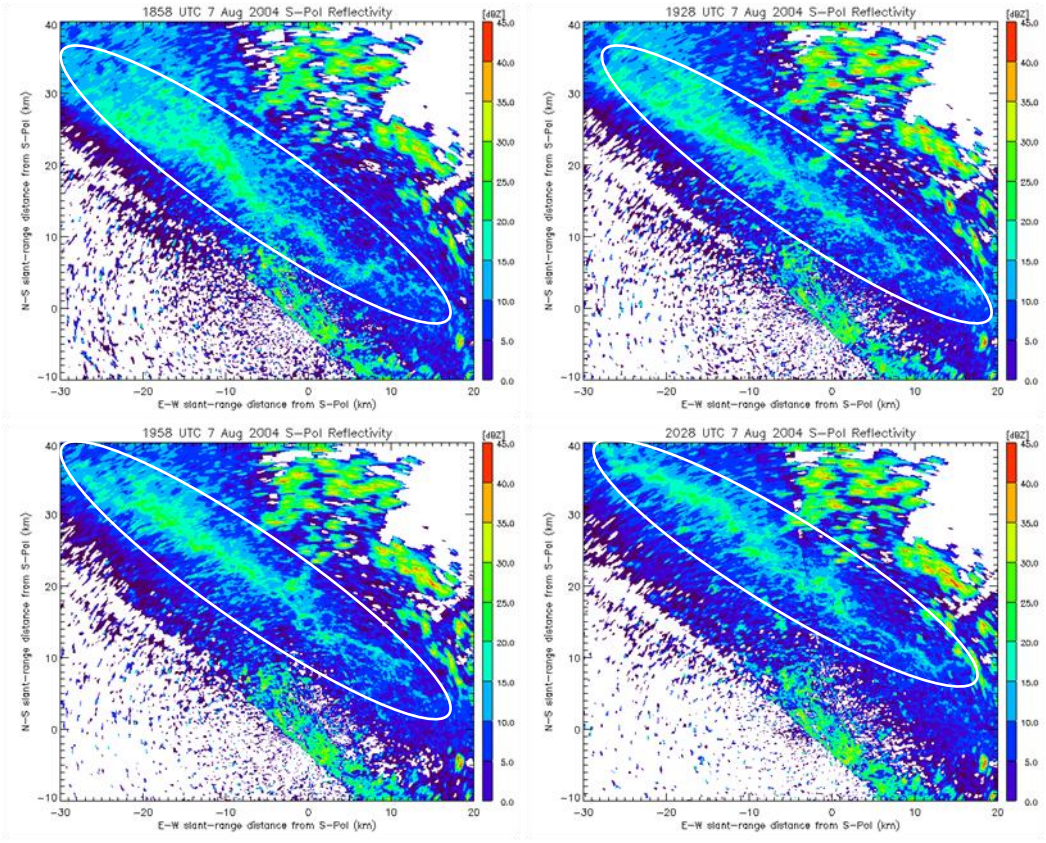

Figure 4.2: As is Figure 4.1, but for 7 August 2004.

4.3 Vertical Structure

4.3.1 Reconstructed RHIs

While PPI scans of the S-Pol data can reveal much information about horizontal structure and intensity of sea breeze fine lines, it is also desirable to gain knowledge of their vertical structure. In the ideal case, S-Pol would have conducted range-height indicator (RHI) scans perpendicular to the sea breeze front. While many actual RHIs were taken during NAME, none of these scans were directed through the sea breeze front.

This was because radar scientists at the time were focusing on convection and structure of precipitation storms, rather than clear air features.

Since no RHIs were available for sea breeze cases, RHIs were reconstructed using 3-D PPI scan volumes. The 3-D PPI data were interpolated to a Cartesian grid from which the reconstructed RHI section was extracted. Fields of interest for RHIs were reflectivity, differential reflectivity, and radial velocity. It was expected that as the leading edge of the sea breeze collected scatterers such as insects, reflectivity would be enhanced in the vertical as was observed in the horizontal on PPI scans. The height of the reflectivity enhancement could then provide information about the depth of the sea breeze. Additionally, it was thought that radial velocity would indicate a discontinuity at the leading edge of the sea breeze. A convergence signature in the radial velocity field would also be expected along the sea breeze.

Differential reflectivity (ZDR) is a measure of the (log) ratio of horizontal reflectivity to vertical reflectivity, and is given by the equation

$$ZDR = 10 \log_{10} (Z_H/Z_V) \qquad [4.2]$$

where Z_H is the reflectivity factor for horizontal polarization and Z_V is the reflectivity factor for vertical polarization. Thus, large oblate scatterers such as insects would be expected to have significant positive ZDR values in excess of 4-5 dB (Wilson et al. 1994). Large raindrops also have a positive ZDR value for the same reason, but these values are typically smaller than the ZDR values associated with insects since raindrops are less oblate. At the leading edge of the sea breeze front, where a concentration of clear-air scatterers are expected, a large positive ZDR value should be observed if insects are the primary scattering mechanism as opposed to precipitation.

A sample of the reconstructed RHIs is shown in Figure 4.3, from 30 July 2004. S-Pol PPI scans from 0.0° through 6.7° were used to create this RHI. PPI data from this case was previously shown in Figure 4.1. The azimuth chosen for this RHI was 45° (with 0° referring to north). This angle was chosen because it was roughly perpendicular to the coast and the sea breeze as seen in the S-Pol PPI scans. The top image in Figure 4.3 shows reflectivity. The sea breeze at this time is located roughly 15 km from the radar (marked with red arrows). While there is a reflectivity maximum of about 10 to 15 dBZ at this location in Figure 4.3, it is difficult to distinguish this from other similarly strong areas, such as that near 43 km from the radar. The sea breeze fine line did not stand out in the RHI reflectivity field as hoped, and can only be pinpointed by comparing Figure 4.3 with the PPI images from Figure 4.1.

In examining the RHI ZDR field, a similar problem presents itself. High ZDR values, in excess of 10 dB in some areas, fill much of the echo area below 3 km. Hence, it is impossible to isolate a single maximum of ZDR values associated with the leading edge of the sea breeze.

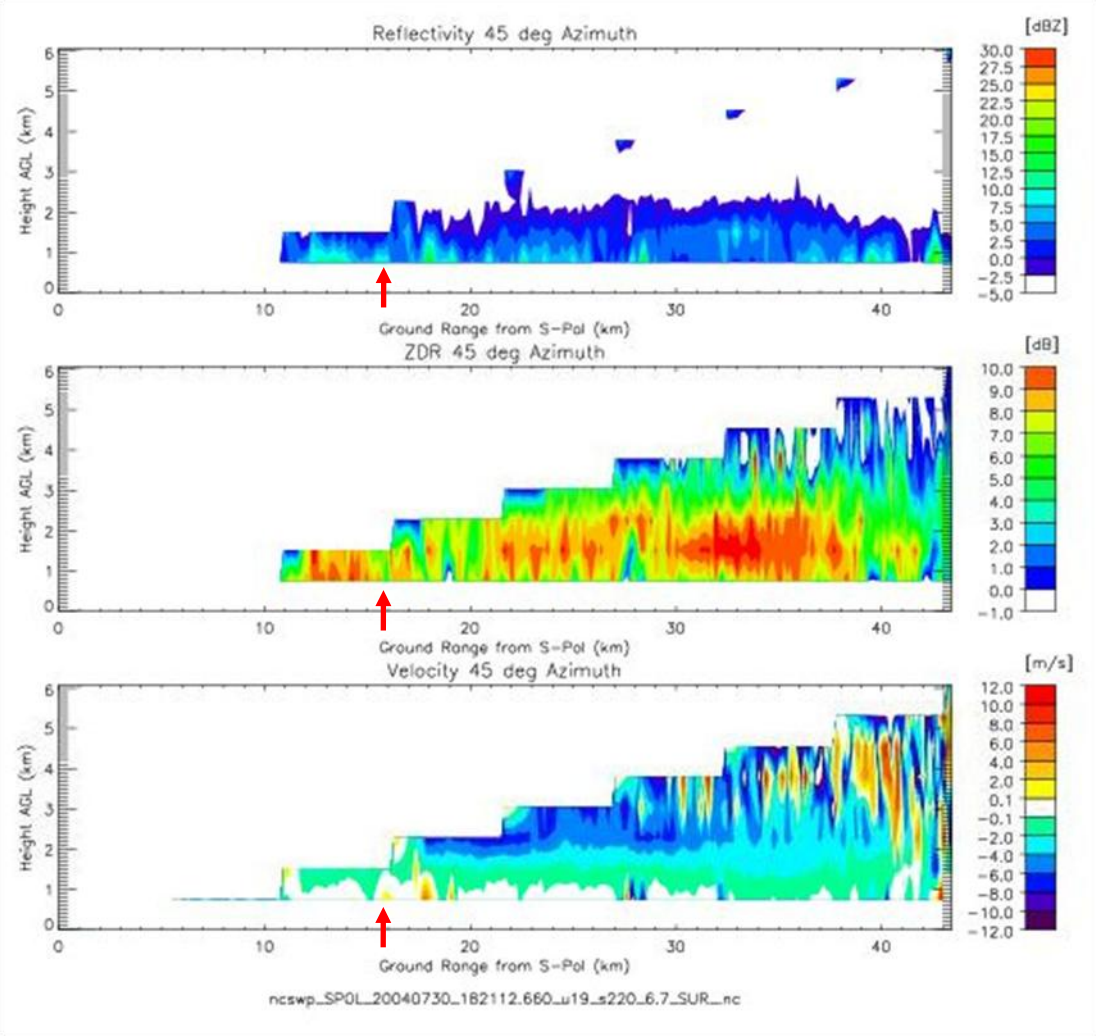

Figure 4.3: Reconstructed S-Pol RHIs of reflectivity, differential reflectivity (ZDR), and radial velocity for 1821 UTC on 30 July 2004, at an azimuth of 45°. Red arrows indicate location of sea breeze fine line.

Figure 4.4 shows a reconstructed RHI from the 7 August 2004 case. The volume scan used for the RHI corresponds to the 2028 UTC 0.0° PPI scan shown in Figure 4.2. At this time, the sea breeze fine line was located roughly 15 km from the radar (at an azimuth of 45°). While the entire fine line is significantly strong in the PPI scans, at the 45° azimuth it is slightly weaker and thinner than the rest of the line. In the reconstructed

RHI, the sea breeze shows up as a slight increase in reflectivity of around 10 to 15 dBZ 15 km from S-Pol. The location is indicated in Figure 4.4 with red arrows. Compared to the 30 July 2004 case presented in Figure 4.3, this sea breeze is a bit easier to see in the reconstructed RHI.

Velocity patterns in Figure 4.4 are unenlightening, as only very weak outbound velocities less than 2 ms^{-1} are found at the sea breeze front location, rather than showing a significant outbound velocity or convergence signature at the leading edge of the sea breeze. ZDR values for the sea breeze location in the RHI range from 5 dB to upwards of 10 dB. However, like the 30 July 2004 case, high ZDR values are present throughout the lower atmosphere, rather than concentrated solely at the leading edge of the sea breeze. This structure, as well as presence of the high ZDR values throughout the lower atmosphere could be due to thermals distributing insects throughout the boundary layer. Since ZDR values were found to be much higher than originally expected, and not only high at the edge of the sea breeze, an investigation into the scattering mechanism for these radar echoes was undertaken.

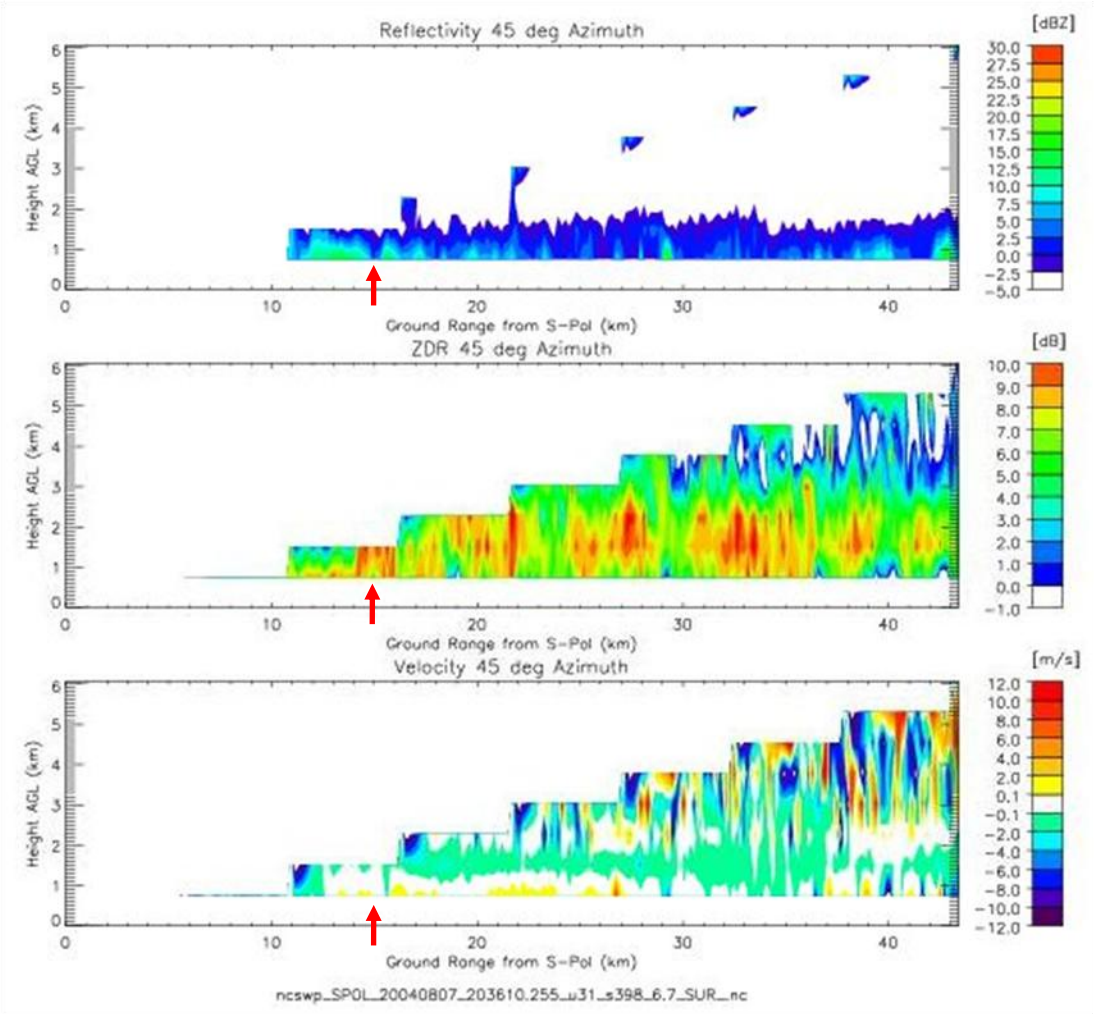

Figure 4.4: Reconstructed S-Pol RHIs of reflectivity, differential reflectivity (ZDR), and radial velocity for 1936 UTC on 7 August 2004, at an azimuth of 45°. Red arrows indicate location of sea breeze fine line.

4.3.2 Refractivity Calculations

In order to investigate the origin of radar echoes seen by the radar, it is necessary to determine the type of electromagnetic scattering taking place. Typically, weather radars, especially S-band radars such as S-Pol, observe precipitation by measuring Rayleigh backscattering from precipitation particles. However, since this study mainly observes clear-air echoes in which no precipitation particles are present (there was no detectable precipitation echoes seen along the sea breeze save for an occasional light shower), any Rayleigh scattering that occurs would likely be due to insects. Bragg scattering due to strong atmospheric gradients in the index of refraction is also a possibility. In order to determine whether or not refractivity gradients were in place to cause Bragg scattering, sounding data was used to calculate atmospheric refractivity. Refractivity in the troposphere is a function of moisture and temperature, and is given by the equation

$$N = \frac{77.6}{T}\left(p + 4{,}810\frac{e}{T}\right) \qquad [4.3]$$

where N is refractivity in N-units, T is temperature in Kelvin, p is pressure in millibars, and e is vapor pressure in millibars (Battan 1959). Since the soundings do not directly measure vapor pressure, saturation vapor pressure was first calculated. The saturation vapor pressure over water is given by

$$e_s = 6.11 \exp\left[a\frac{(T-273.16)}{(T-b)}\right] \qquad [4.4]$$

where e_s is saturation vapor pressure in millibars, T is temperature in Kelvin, and a and b denote constants that are different for ice and water (Garand et al. 1992). The values of a

are 17.269 and 21.875 for water and ice, respectively. The values of b are likewise 35.86 and 7.66 for water and ice, respectively.

Once saturation vapor pressure was determined, relative humidity was calculated using

$$RH_{w/i} = \frac{[e_{s,w}(T_d)]}{[e_{s,w/i}(T)]} * 100 \quad [4.5]$$

where $RH_{w/i}$ is the relative humidity with respect to water or ice, $e_{s,w}$ is saturation vapor pressure with respect to water, $e_{s,w/i}$ is the saturation vapor pressure with respect to water or ice, T_d is the dew point temperature in Kelvin, and T is the temperature in Kelvin. The soundings did not report relative humidity directly. However, since relative humidity is also given by

$$RH = \frac{e}{e_s} * 100 \quad [4.6]$$

the saturation vapor pressure (e_s) and relative humidity (RH) can be used to calculate the vapor pressure, e. Once the vapor pressure is known, refractivity can be calculated using the equation [4.3].

Soundings from two stations, the ship Altair and the land station at Mazatlán, are used to compare the refractivity over water with that over land. Figure 3.1 shows the location of both Mazatlán and the Altair. Ideally, these locations were taken to represent the two different atmospheric environments separated by the sea breeze front. Air behind the sea breeze would typically be cooler and more moist than the air located over land, ahead of the approaching sea breeze. In a situation where the land-sea thermal contrast is strong, one would expect to see a significant difference between refractivity values over land and water.

Furthermore, the amount of variation between refractivity values between land and water will provide evidence as to the type of scattering that is leading to the echoes observed by S-Pol. If refractivity in the near-surface layer is found to differ significantly between the sea sounding (Altair) and the land sounding (Mazatlan), Bragg scattering by variations in the index of refraction could be a cause for the observed radar echoes. However, if the difference in refractivity values between the two locations is minimal, Rayleigh scattering from insects is likely dominant.

Figures 4.5 and 4.6 show sounding data from the Altair and Mazatlán upper air sites for 7 August 2004. These soundings were taken around 12 UTC (exact times shown in the figures), which was prior to the time sea breeze front had moved onshore. This time was chosen so that the Altair sounding would be representative of the marine air mass, located westward of the sea breeze front. Mazatlán would at this time be representative of the land air mass, ahead of the sea breeze front. Soundings at 18 UTC were available for some cases, however the sea breeze front had usually moved onshore and past the Mazatlán sounding site by this time, so both the Altair and the Mazatlán soundings would be representative of the ocean air. Figure 4.5 shows refractivity in N-units calculated using the previously described method. Values are around 280 units at the surface, and decrease somewhat steadily through higher parts of the troposphere. Values are shown only from the surface through 800 mb since effects of the thermal contrast across the sea breeze front would be much less higher up in the troposphere. As is evident in Figure 4.5, refractivity is nearly equal for the two locations at the surface, with only a slight difference in the layer from about 970mb – 900 mb.

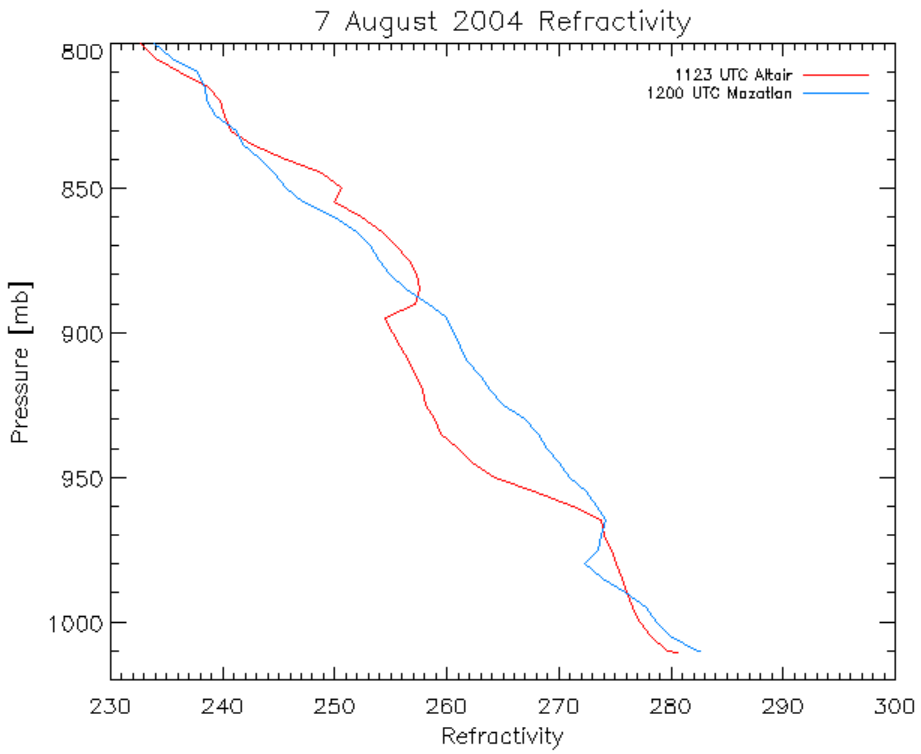

Figure 4.5: Refractivity in N units calculated from the Altair and Mazatlan soundings for 7 August 2004.

Figure 4.6 shows temperature and dewpoint data from the same soundings. As would be expected from the refractivity displayed in Figure 4.5, values of temperature and dewpoint are also very similar for the two locations. The dewpoint temperature for the Altair sounding is about 4 to 5 degrees lower in the layer from 970 mb through about 900 mb, which would explain why the refractivity was also lower in this layer. However, overall there seems to be very little contrast between the air over the ocean and the land-based air. This lack of refractivity difference implies that it is not Bragg scattering from strong refractivity gradients that is leading to radar echo along the sea breeze front.

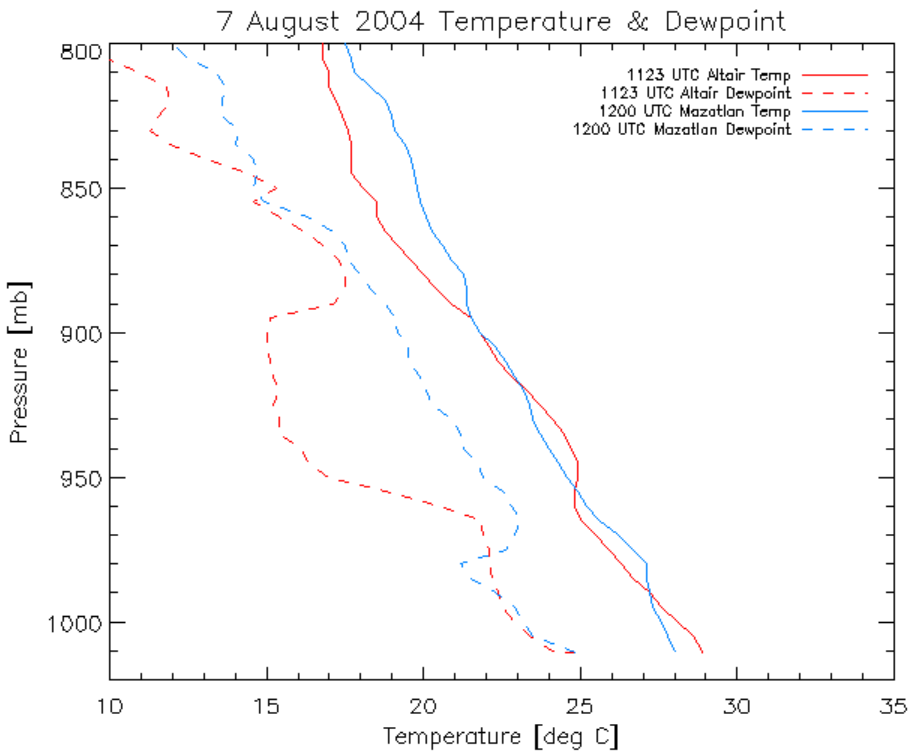

Figure 4.6: Temperature and dew point temperature from the Altair and Mazatlan soundings for 7 August 2004.

Ralph (1995) provides a method for determining if radar echoes are due to Bragg scattering from changes in refractivity or Rayleigh scattering from hydrometeors or insects. Figure 4.7, from Ralph (1995) shows thresholds of scattering detection for various radar wavelengths. S-Pol is an S-band radar with a wavelength of approximately 10 cm, and would correspond to the line labeled "3 GHz (10 cm)". This line indicates the amount of Rayleigh scattering, measured in dBZ, equivalent to a given amount of Bragg scattering, represented by the structure parameter C^2_n. Higher values of C^2_n indicate more turbulence necessary in the atmosphere to produce a certain level of Bragg scattering.

By looking at the line that corresponds to S-band radars, we can determine what values of reflectivity from S-Pol would be realistic for Bragg scattering, and which can

only be caused by Rayleigh scattering. Since the shaded area represents the transition from Bragg-dominated scattering to Rayleigh-dominated scattering, we can use the intersection of the 10 cm line with the edges of the shaded bar to determine transition values in terms of dBZ. The 10 cm line intersects the lower boundary of the shaded area at about -35.4 dBZ. This means that any reflectivity values below -35.4 dBZ are likely caused by Bragg scattering mechanisms. Likewise, the 10 cm line intersects the top boundary of the shaded area at a value of about -15.4 dBZ. Any reflectivity values measured above -15.4 dBZ could only be due to Rayleigh scattering off of particulate matter such as hydrometeors or insects, since an extreme level of turbulence, which Ralph labels as "rarely occurs", would be required to cause such high reflectivity values from Bragg scattering mechanisms. In between these two values of -35.4 dBZ and -15.4 dBZ, or what would fall within the shaded area in Figure 4.7, either Bragg or Rayleigh scattering could be responsible for the echo on the radar display.

PPI scans examined in section 4.2 have already shown that the reflectivity values measured in the sea breeze fine line are well above the threshold of -15.4 dBZ. Reflectivities of 5 to 20 dBZ as were observed during NAME could not be caused by Bragg scattering, so it must be concluded that the primary scattering mechanism for sea breeze features during NAME is Rayleigh scattering. Since ZDR values were found to be so high, it is more than likely that the scatterers for sea breeze fine lines during NAME are large insects. Furthermore, since ZDR values were not only high at the sea breeze front but throughout the boundary layer, we conclude that insects were abundant in NAME and this was a primary reason in why the sea breeze front was not readily detectable with reflectivity or differential reflectivity.

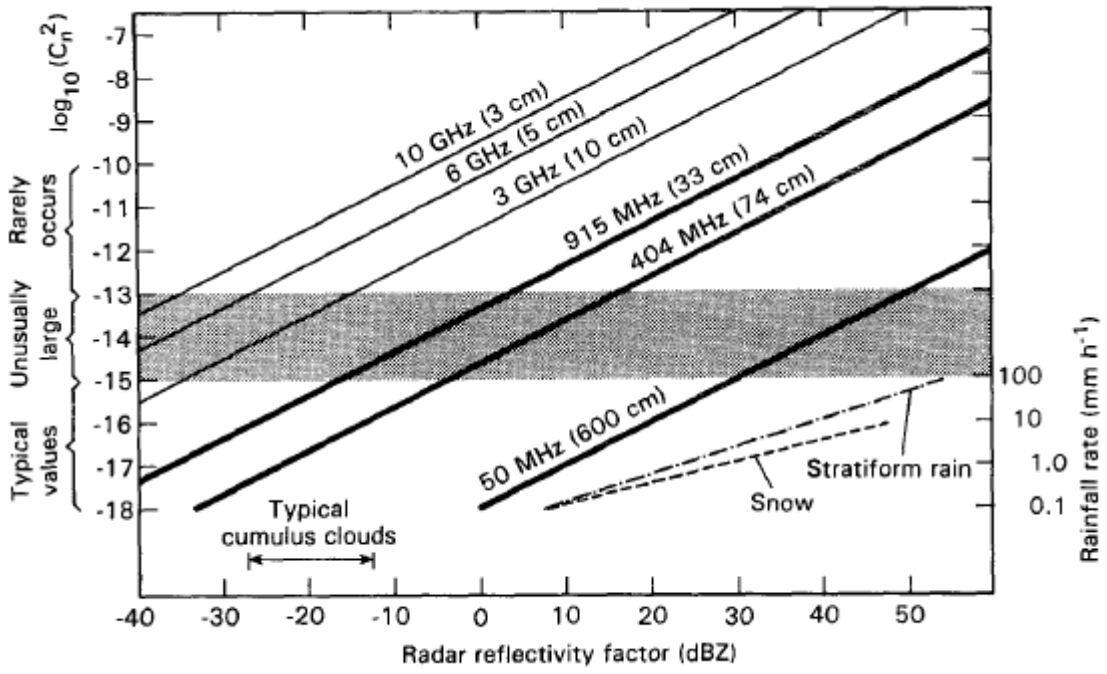

Figure 4.7: Regime diagram for Rayleigh scattering vs. Bragg scattering for various radar wavelengths. Lines indicate the amount of Rayleigh scattering that is equivalent to a given amount of Bragg scattering. The shaded area represents the transition from Bragg-dominated scattering to Rayleigh-dominated scattering. [from Ralph (1995)]

4.3.3 Wind Profiler Analysis

Since reconstructed RHI plots from S-Pol data did not provide much information about the vertical structure of the sea breeze front, NAME wind profiler data were analyzed to examine sea breeze structure. As described in Chapter 3, wind profiler data was obtained from the 915 MHz wind profiler located at Estación Obispo. While not a scanning radar like S-Pol, the vertically pointing radiation from ETO will provide a single point's view of the sea breeze front as it passes over the wind profiler's location. Time-height plots were generated using the wind profiler's reflectivity field, which are similar in some ways to the reconstructed RHI plots. The reflectivity from the profiler

was not calibrated, and therefore will be referred to as "relative" reflectivity. When precipitation was present, the vertical velocity represents the fall speed of precipitation particles. In the absence of rain, the 915 MHz profiler measured vertical velocity directly. A reflectivity maximum would be expected at the time of the sea breeze front passage, as scatterers are caught in the advancing edge of the sea breeze. In the vertical velocity field, an area of positive velocities would be expected at the leading edge of the sea breeze as the cooler moist air behind the sea breeze front lifts the land-based warmer and drier air mass.

Figure 4.8 shows ETO profiler relative reflectivity and vertical velocity for 7 August 2004. The black vertical line on each of the plots indicates the approximate time of the sea breeze front passage over the ETO station. The time of the SBF passage was determined from surface wind direction data in combination with PPI images of reflectivity from S-Pol. Surface wind direction for 7 August 2004 is shown in Figure 4.9. The surface winds shifted from variable northerlies to westerlies at about 2130 UTC, coincident with the passage of a reflectivity fine line identified by S-Pol.

At the approximate time of sea breeze passage, 2130 UTC, an enhancement is seen in the relative reflectivity field in Figure 4.8. Values at this time are about 15 – 25 dBZ, compared with the background of around -5 to 5 dBZ. The velocity field indicates upward vertical velocities are present with peak values to about 1.5 ms^{-1}. However, this positive vertical velocity is not distinguishable from the other vertical velocity maxima present at approximately 1930 UTC, 2000 UTC, and 2040 UTC. Rather than showing an obvious positive vertical velocity signal at the time of sea breeze front passage, the

vertical velocity field reveals a periodicity of updrafts and downdrafts that repeat about every 30 to 60 minutes, suggesting a wave-like structure.

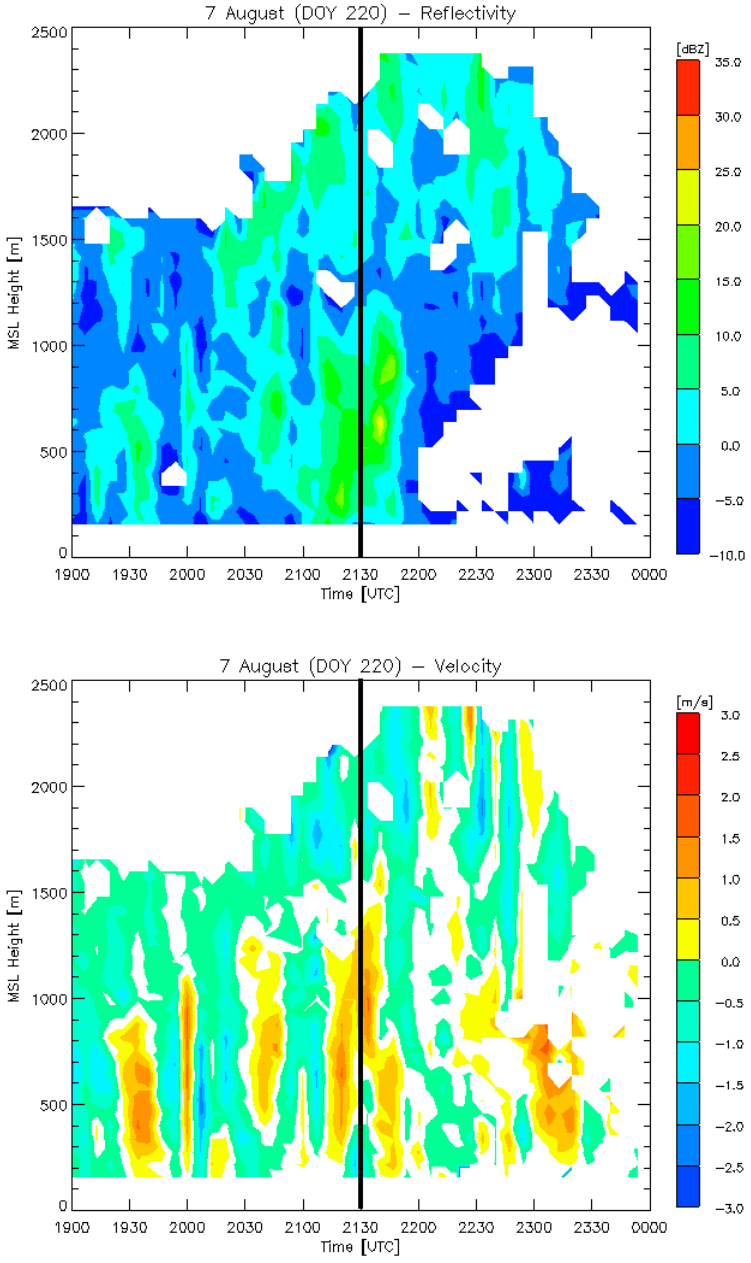

Figure 4.8: Estación Obispo 915 MHz wind profiler relative reflectivity (top) and vertical velocity (bottom) on 7 August 2004. Black vertical line indicates approximate time of sea breeze front passage over the ETO station.

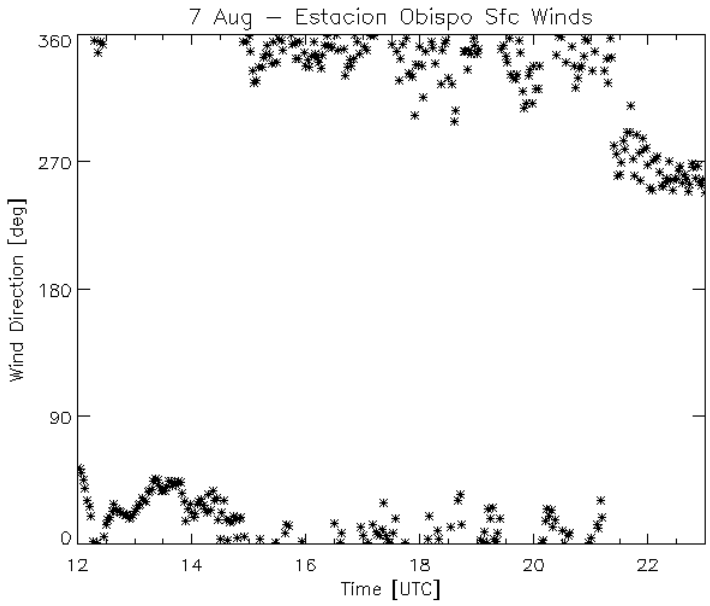

Figure 4.9: Wind direction from the Estación Obispo surface station for 7 August 2004. 0° and 360° correspond to northerly winds, 90° to easterly winds, 180° to southerly winds, and 270° to westerly winds. Data resolution is every 2 minutes.

This velocity pattern of periodic updrafts and downdrafts was seen for several cases examined. Figure 4.10 shows another example of this structure, from 10 August 2004. On this day, sea breeze front passage over ETO occurred around 1730 UTC, which is marked on the images. In the reflectivity field, there is a slight maximum of around 20 dBZ seen at time of sea breeze front passage, but a larger much more obvious reflectivity maximum occurs later, around 1800 UTC. It is possible that this reflectivity maximum is not due to the passage of the sea breeze at all. At the location of the profiler (331.6° azimuth and 44.6 km range from S-Pol), the 0.8° S-Pol elevation scan reaches about 3 km above the ground, which corresponds to the height of the reflectivity maximum seen by the profiler. Examination of the S-Pol data at this point, marked by a white oval in Figure 4.12, reveals that ZDR values over the profiler site at this time are near 0, and reflectivity values are very low. These values point to a small cloud being detected by

the profiler, rather than insects lofted by the sea breeze front, since insects would have a high ZDR. The surface wind direction for 10 August 2004, shown in Figure 4.11 reveals that the wind shift associated with the sea breeze passage was not as sudden as on 7 August 2004. The wind direction shifted to southwesterly around 1730 UTC, but remained variable. The direction then becomes steadier just after 1800 UTC. Thus, the exact time that the sea breeze front passed over ETO was difficult to determine.

The velocity pattern for 10 August 2004 reveals a similar situation to that of 7 August 2004. At the marked time of sea breeze passage, 1730 UTC, there is a very slight upward vertical velocity of about 0.5 ms^{-1}. However, just after the sea breeze front passage, at 1800 UTC, there is a much larger positive vertical velocity value of around 2 ms^{-1}. Overall, the vertical velocity pattern on 10 August 2004 is similar to that of 7 August 2004 shown in Figure 4.8. The vertical velocity again shows a pattern of upward and downward motion, this time repeating about every 30 minutes.

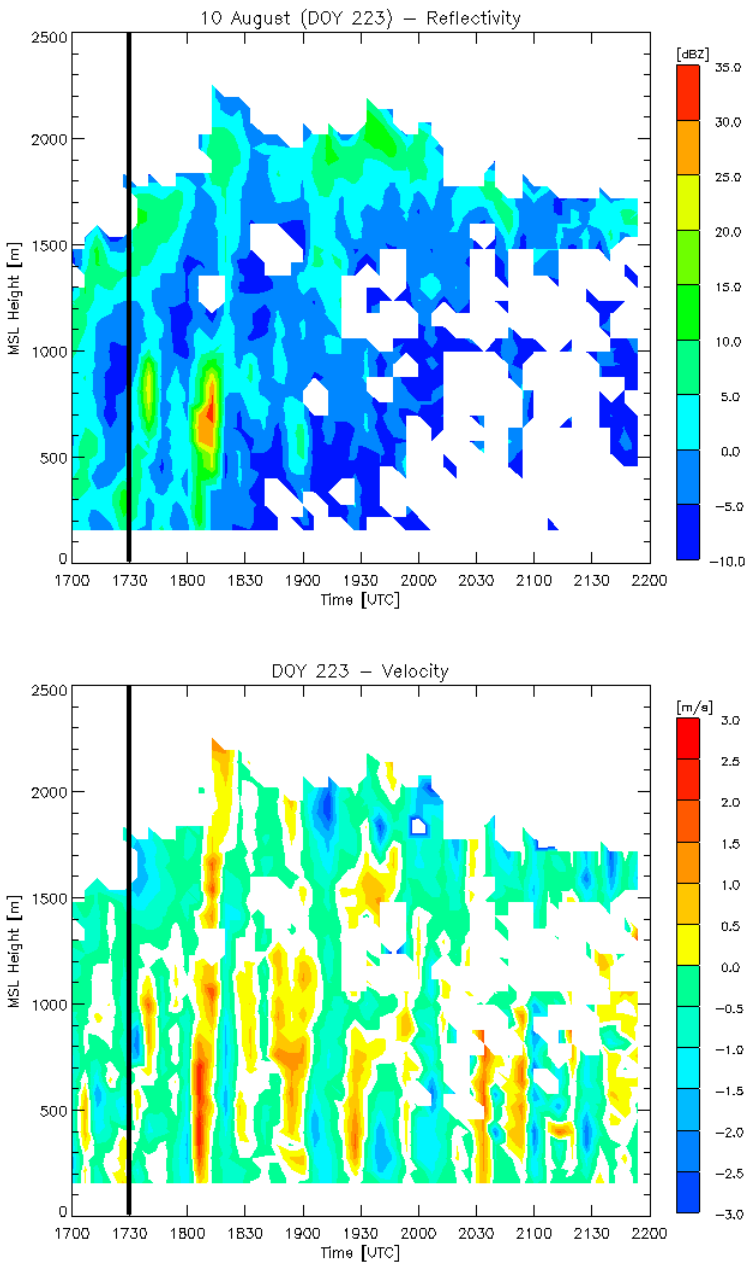

Figure 4.10: As in Figure 4.7, but for 10 August 2004. Note that the times are slightly different than those shown in Figure 4.6.

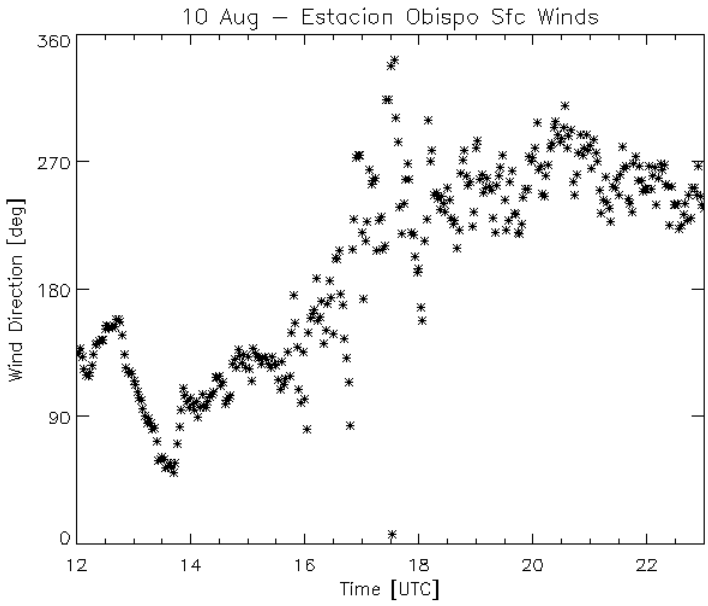

Figure 4.11: As in Figure 4.8, but for 10 August 2004.

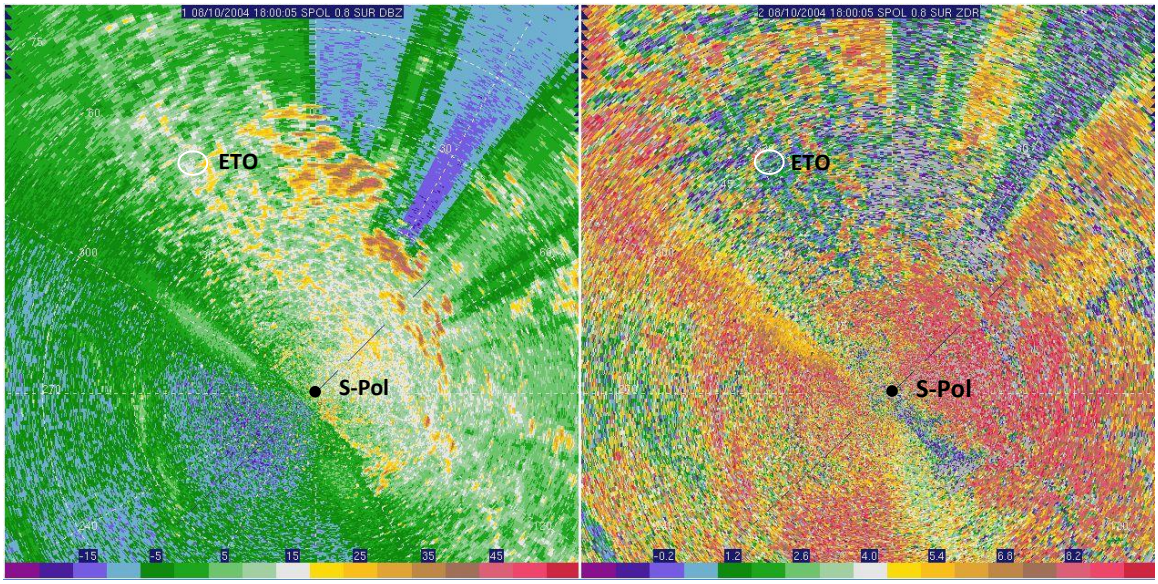

Figure 4.12: S-Pol reflectivity in dBZ (left) and ZDR in dB (right) for 1800 UTC on 10 August 2004. PPI shown is at an elevation angle of 0.8°. S-Pol and profiler (ETO) locations are indicated. White oval denotes area directly over the profiler site.

Profiler relative reflectivity and vertical velocity data for 17 August 2004 are shown in Figure 4.13. Unlike the previous two cases that were presented, the sea breeze signature in this case is nearly undetectable. Sea breeze front passage over ETO is marked at 1900 UTC. In the relative reflectivity data, there is a "maximum" of between 0 and 5 dBZ at this time, but it is no greater than the reflectivities from 1700 UTC through 1800 UTC, or from 2000 UTC through 2100 UTC at around 1500-2000 m above the ground. Vertical velocity shows slight upward motion at 1900 UTC of up to 1.5 ms^{-1}. However, stronger positive vertical motion is actually present earlier at 1700 UTC and 1800 UTC.

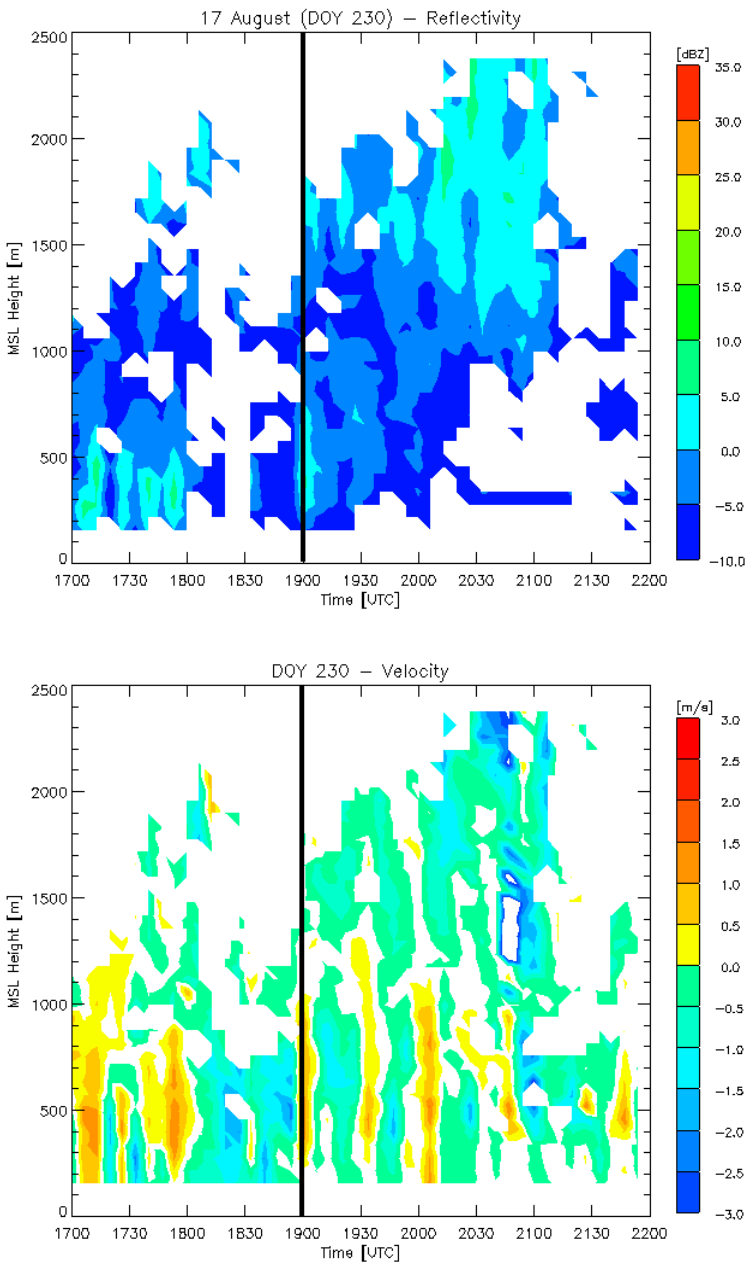

Figure 4.13: As in Figure 4.7, but for 17 August 2004.

One explanation for such weak sea breeze front signatures in the profiler data for 17 August 2004 could be that the sea breeze on this day was simply weaker than on other days during NAME, owing to small thermal contrast between land and sea. In terms of reflectivity strength, the fine line observed on S-Pol for this day is not as prominent as in

other NAME cases. S-Pol data shown in Figure 4.14 reveals a weak fine line, but nonetheless indicates the presence of a sea breeze on this day. The sea breeze is even more noticeable when PPI images are viewed in a video loop. Surface wind direction is shown in Figure 4.15. Surface wind data, however, does not seem to indicate that this sea breeze is weak. Unlike other cases, there is an obvious wind shift at 1900 UTC from widely variable winds to steady winds out of the southwest, just as would be expected as a sea breeze moves onshore.

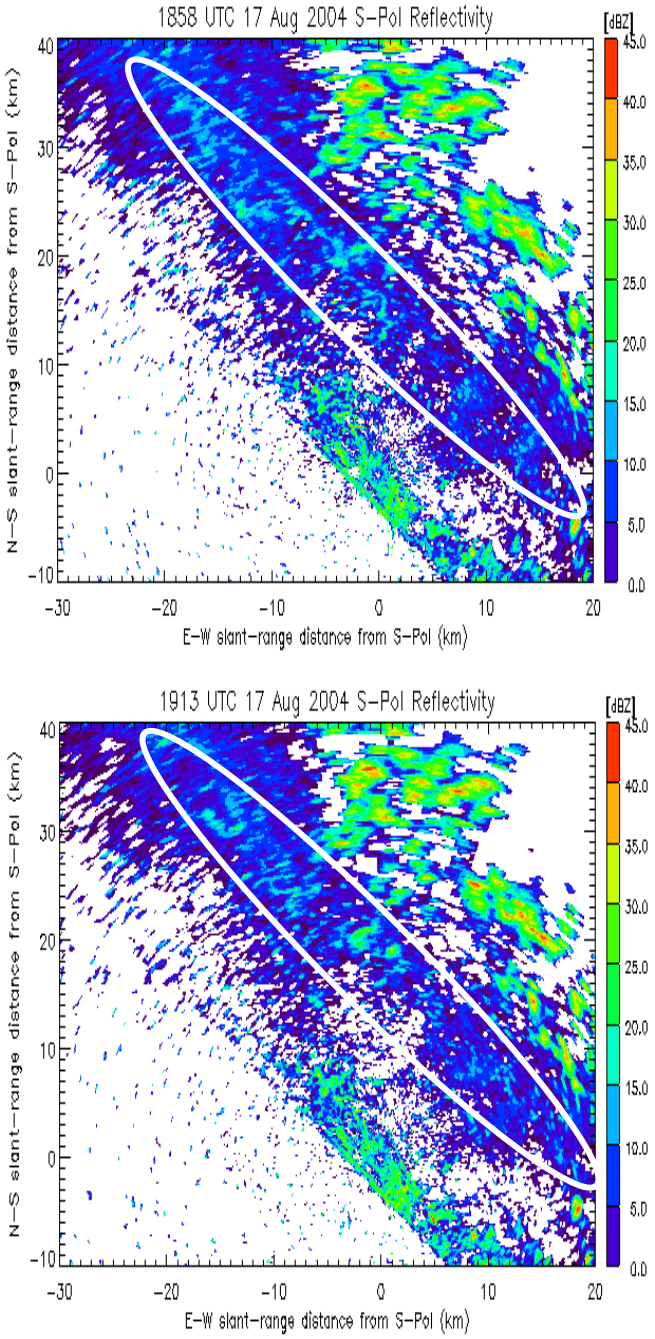

Figure 4.14: S-Pol PPI reflectivity for 17 August 2004. Times are displayed on each individual image. Scans shown are at an elevation angle of 0.0°. Axes are displayed as slant-range distance (km) from S-Pol, which is located at (0,0). White ovals in each frame indicate the sea breeze fine line.

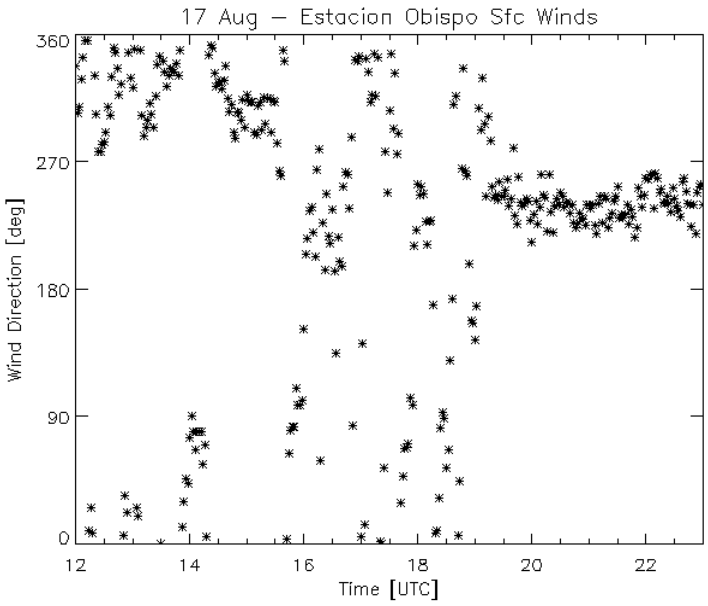

Figure 4.15: As in Figure 4.9, but for 17 August, 2004.

While wind profiler reflectivity and velocity data does provide more information about the vertical structure of the sea breeze front than reconstructed RHIs from S-Pol, the sea breeze signature is difficult to distinguish from other boundary layer features. In hopes of gathering more information about the vertical structure of the leading edge of the sea breeze, time-height plots of horizontal winds were constructed using the ETO profiler data. The goal of this type of analysis is to show air movement throughout the boundary layer, rather than just at the surface.

Figure 4.16 shows profiler-derived horizontal winds for 7 August 2004. Times are displayed in UTC. Wind barbs have been created to show wind direction at individual points throughout the boundary layer. As with the surface winds discussed previously, winds out of the West would be expected as the sea breeze front moves over the ETO station. On this day, winds were mainly out of the North from about 9 UTC, on. Beginning around 2000 UTC, a westerly component appears. Wind vectors with

westerly components in the lower portion of the boundary layer have been outlined in blue. The leading edge of the sea breeze appears to at first extend higher into the atmosphere, up to around 1.5 km. Then as the leading edge passes ETO, winds remain westerly up to about 0.75 km, but regain a northerly component above this level.

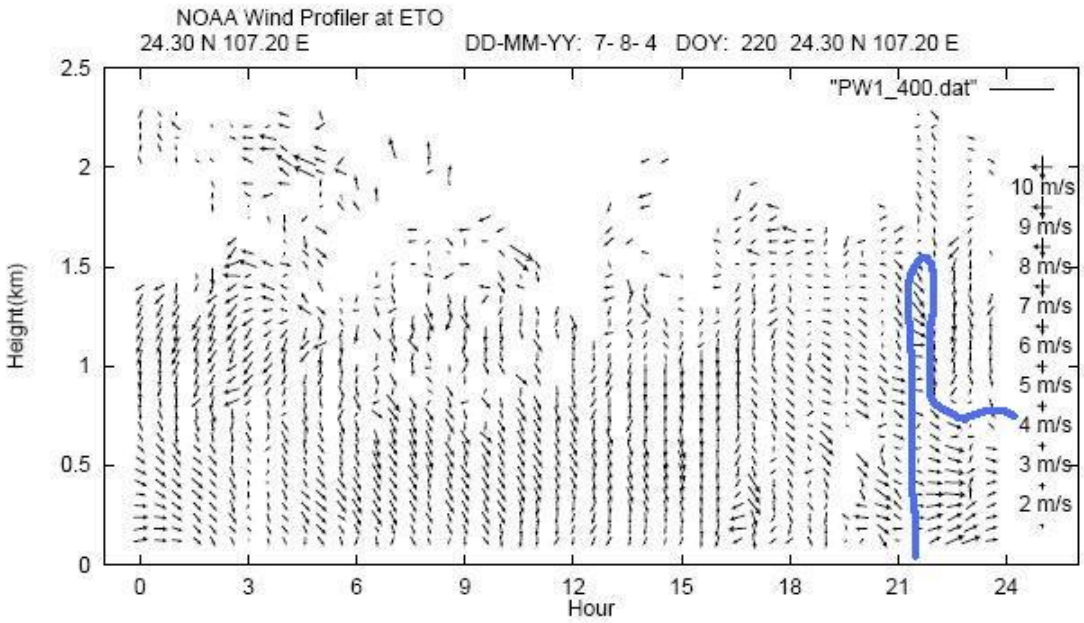

Figure 4.16: Estación Obispo wind profiler wind vectors for 7 August 2004. Time is in UTC. Curved blue line denotes wind vectors with a westerly wind component due to sea breeze passage over ETO.

Figure 4.17 shows wind profiler wind vectors for 10 August 2004. Unlike 7 August 2004, the sea breeze westerlies reach their highest point a couple hours after the initial appearance of westerly winds at the surface. There is also a brief break in westerly winds just before 2100 UTC. The sea breeze height seems similar to the 7 August 2004 case, however, with westerly winds ranging from just under 1 km up to 1.5 km. Wind vectors for 17 August 2004 are shown in Figure 4.18. Like the previous two cases, westerly winds extend from the surface to around 1 km. This case has less variation in

height, however, with the first appearance of westerly winds extending to just above 1 km, and then afterwards extending to slightly below 1 km.

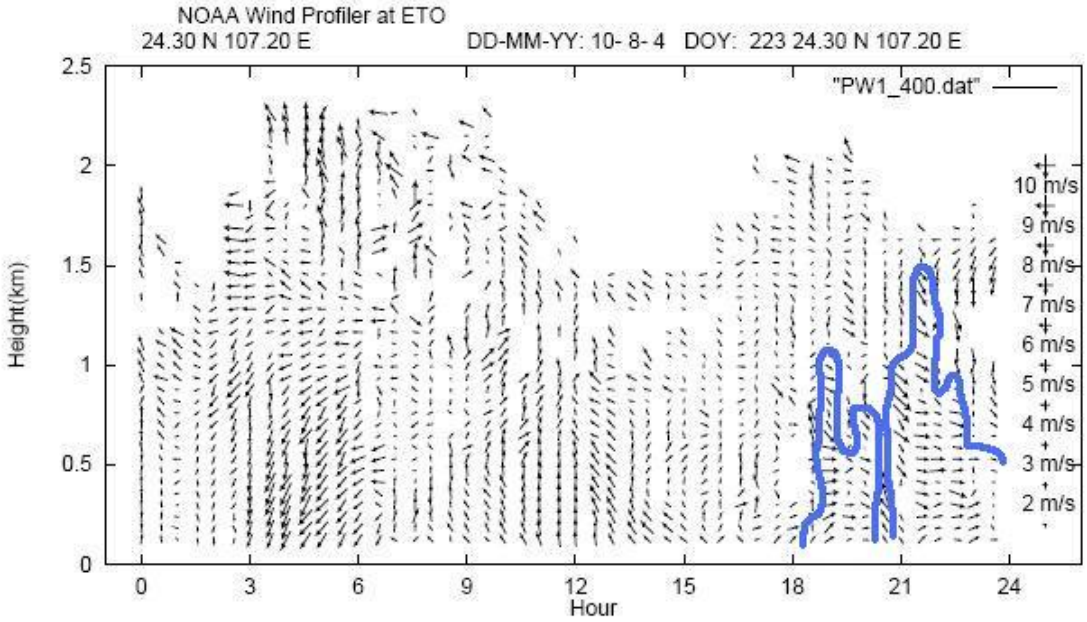

Figure 4.17: As in Figure 4.16, but for 10 August 2004.

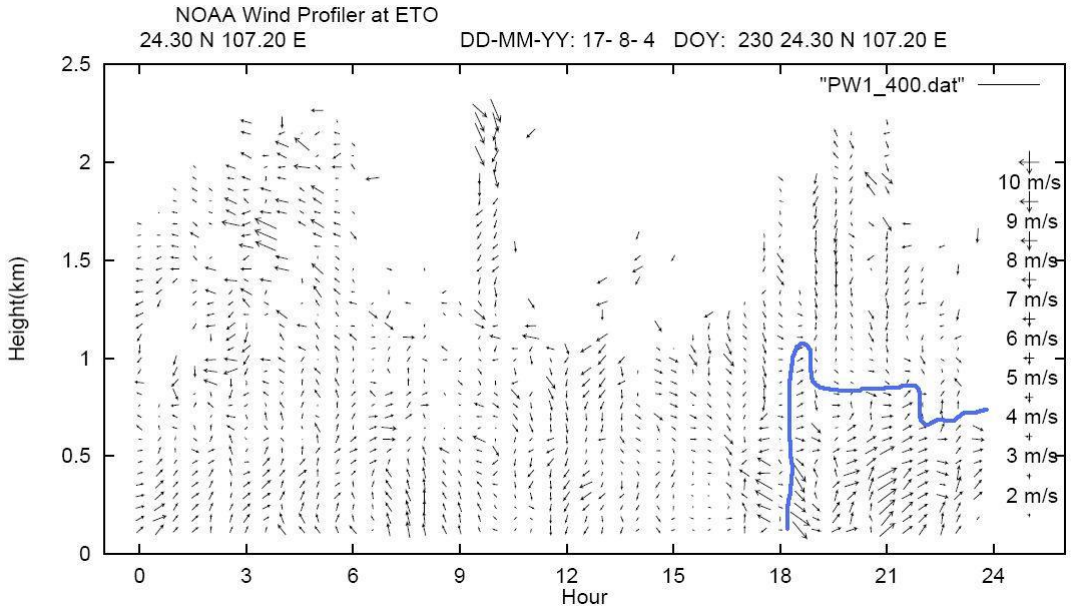

Figure 4.18: As in Figure 4.16, but for 17 August 2004.

The sea breeze "shape" revealed through this wind profiler analysis sometimes resembles that of a density current, with a leading head that extends higher vertically than the area behind it. Figures 4.16 and 4.18 both show this structure. Sha et al. (1991) found a similar structure in numerical model simulations of sea breezes. Wind vectors for one of their sea breezes are shown in Figure 4.19. The solid line indicates the boundary between the ocean air and the land air. The leading edge of this boundary, which represents the leading "head" of the sea breeze, is about 660 m above the ground. The portion of the boundary that follows extends to about half this height, or 320 m.

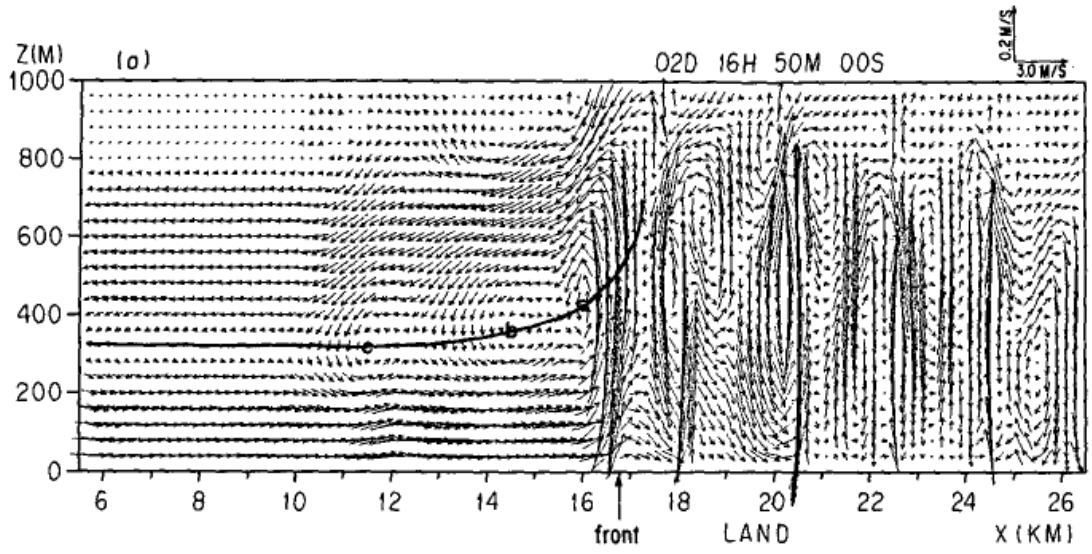

Figure 4.19: Vertical cross section of wind vectors at 1650 LST for a simulated sea breeze. The solid line indicates the zero-velocity boundary. Horizontal axis indicates distance from the coastline. Position of the sea breeze front at the surface is also shown. From Sha et al. (1991).

When comparing the wind vectors from these three cases, it is apparent that the vertical structure of wind direction and magnitude within the sea breeze varies greatly from day to day. Some cases like 10 August 2004 seem more complicated, whereas the sea breeze on 17 August 2004 doesn't seem to vary as much in height. However, overall

the vertical extent of sea breezes in NAME does not seem to reach much above 1.5 km. Some cases, such as 7 August 2004 and 17 August 2004, have structures similar to a density current, with a raised "head" region. Simpson et al. (1977) and Simpson and Britter (1980) were among the first to compare the structure of sea breeze fronts to that of a density current, and the latter found that the height of the leading "head" region was about twice that of the region seaward. The structure in Figure 4.16 from 7 August 2004 is consistent with these findings. What is still surprising is that the profiler data seems to give a better vertical representation of the sea breeze front as it moves onshore compared to the radar data. This is probably a result of the better raw vertical resolution in the profiler data compared to the scanning radar. The original intent of this project was to examine the sea breeze fronts during NAME using radar data. It was thought that the radar reflectivity and vertical velocity would have a signature that stood out from the background features, which could then be examined to gain information about the shape and vertical extent of the sea breeze. However, as has been shown, the reflectivity data proved to marginally useful in revealing the vertical structure of NAME sea breezes. In the sections that follow, the study will aim to explain why the detailed structure of the sea breeze was so difficult to discern using S-Pol radar observations.

4.4 General Boundary Layer Characteristics

As a result of this study focusing on clear-air radar features, insight has been gained into some of the characteristics of the coastal plain atmospheric boundary layer. While the sea breeze fine line signature was not easily detectable with S-Pol, there were certainly plenty of scatterers in the viewing area of this radar. This section will

investigate features (other than sea breezes) of the NAME boundary layer as observed by S-Pol and the ETO wind profiler.

4.4.1 High Differential Reflectivity Values in Radar Data

The abundance of clear-air scatterers became even more obvious when the reconstructed RHIs were created from the S-Pol PPI data. As discussed previously in section 4.3.1, high ZDR values were present throughout the boundary layer. No signal of high ZDR at the leading edge of the sea breeze front was observed as was originally expected. These high ZDR values that were observed prompted an investigation into the scattering mechanisms at work in the boundary layer.

Refractivity calculations from soundings, discussed in section 4.3.2, suggested that the thermal contrast between the land air mass and the ocean air mass was not sufficient to contribute to Bragg scattering. Furthermore the observed reflectivities were much too large to be explained by Bragg scatter. This leaves one to assume that the radar echoes and high ZDR values were due to Rayleigh scattering. However, it is important to understand whether or not the ZDR values measured by S-Pol are realistic. Past radar studies can be used to compare the values of ZDR found in this study with values previously measured in other locations. Lang and Rutledge (2004) observed dumbbell-shaped echoes from insects with ZDR values often greater than 4 dB. The dumbbell appearance of the echoes was caused by the insects being aligned with the mean wind. Thus, when the radar was pointed perpendicular to the mean wind direction, it was observing the long sides of the insects and thus had a higher reflectivity and large ZDR. When the radar was pointed parallel to the direction of the mean wind, the reflectivity

and ZDR were lower. The oblong shape of the insects leads to large positive ZDR values, since horizontal reflectivity is much greater than vertical reflectivity.

Zrnić and Ryzhkov (1998) used a 10 cm wavelength polarimetric weather radar to study biological scatterers. These authors note that while radar echoes from insects rarely have noticeably high reflectivity factors, high positive ZDR values are their distinguishing factor. For one case, ZDR measurements of up to 7 dB were found within the boundary layer when the radar beam was directed perpendicular to the horizontal wind. These results suggest that the radar beam was observing the long side of insects, causing horizontal reflectivity to be much larger than the vertical reflectivity, which resulted in large positive ZDR values. Other similiar studies (Achtemeier 1991, Wilson et al. 1994) have found ZDR values of 8, 9, and even 10 dB within the boundary layer.

Past studies confirm that ZDR values found in this study of 10 dB and occasionally up to 15 dB are not unrealistic for large oblong objects such as insects (Wilson et al. 1994). Since the high ZDR values are so widespread, rather than concentrated at the leading edge of the sea breeze, it is difficult to use radar data alone to study the vertical structure of the sea breeze. However, such prevalent high ZDR values in the boundary layer confirms that there is an abundance of scatterers, most likely insects, that is rendering the sea breeze signal difficult to distinguish from the background reflectivity.

4.4.2 Horizontal Convective Rolls

Another interesting boundary layer feature that was observed is the presence of what is thought to be horizontal convective rolls. The profiler data were used to

investigate the vertical air motion as sea breezes passed over ETO, in hopes of finding a single dominant positive vertical velocity signature associated with the sea breeze front. Instead, many of the cases examined showed periodic updrafts and downdrafts within the boundary layer. An excellent example of this structure was found on 17 August 2004 was (Figure 4.13). The presence of multiple distinct updrafts made it difficult to distinguish which particular updraft was due to the sea breeze front. These periodic updrafts and downdrafts suggested that some sort of (periodic) feature besides the sea breeze front was present in the boundary layer. Wind profiler data was further examined for this behavior during the evening and night time hours. However, during none of these cases was any periodic updraft and downdraft activity observed during nighttime hours. Since the periodic behavior was only observed during the daytime when solar heating was present, it is extremely likely that the cause is tied to diurnal heating. Thus, the most likely explanation for this periodicity in the vertical velocity is the presence of horizontal convective rolls.

Once this behavior was observed in the wind profiler data, a second look at S-Pol data revealed that occasionally the reflectivity field also supported the presence of convective rolls. Figure 4.20 shows S-Pol reflectivity (left) and radial velocity (right) for 17 August 2004. S-Pol reflectivity data reveals a pattern of NW-SW oriented fine lines just north of the radar, with reflectivity values of about 20 dBZ. These fine lines appeared much earlier compared to when the sea breeze fine line first appeared. The image in Figure 4.19 is for 1522 UTC, whereas the sea breeze fine line on this day did not appear until around 1800 UTC.

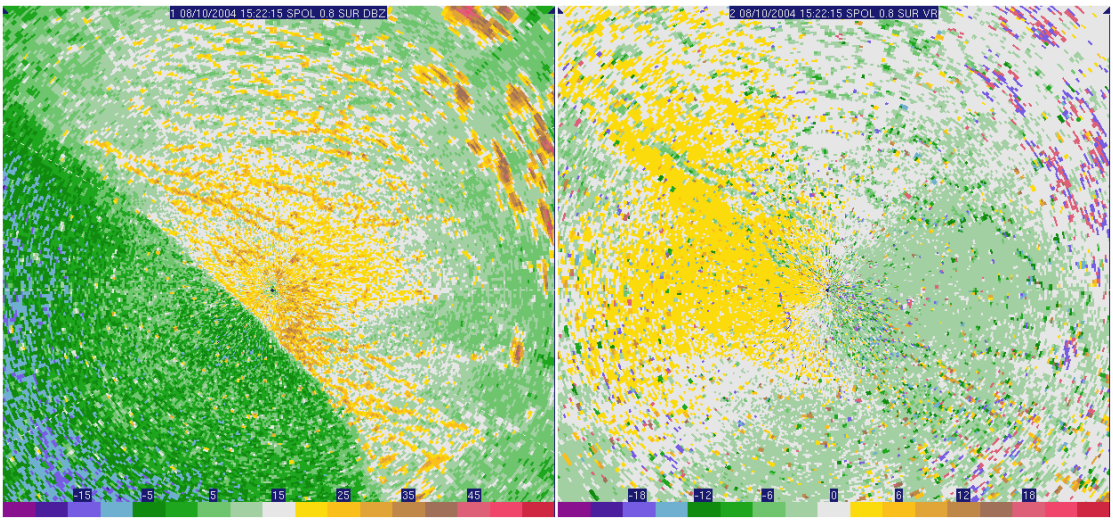

Figure 4.20: S-Pol reflectivity and radial velocity at an elevation angle of 0.8° for 1522 UTC on 17 August 2004. Reflectivity is in units of dBZ and radial velocity is in units of ms^{-1}.

Previous studies have investigated the characteristics of horizontal convective rolls. Often, the boundary layer height is compared to the wavelength of the convective rolls through the aspect ratio. The aspect is defined as

$$A = \frac{\lambda_{ROLL}}{Z_i}$$

Where A is the aspect ratio, λ_{ROLL} is the roll wavelength, and Z_i is the boundary layer depth. Previous research has found HCR aspect ratio values of 2.8 (Kuettner 1971), 2.2-6.5 (LeMone 1973), and 5.7 (Weckwerth et al. 1997). It has also been shown that a higher aspect ratio indicates an environment with greater thermal instability (Weckwerth et al. 1997). Figure 4.21 illustrates the relationship between boundary layer depth and roll wavelength measured by Weckwerth et al. (1997).

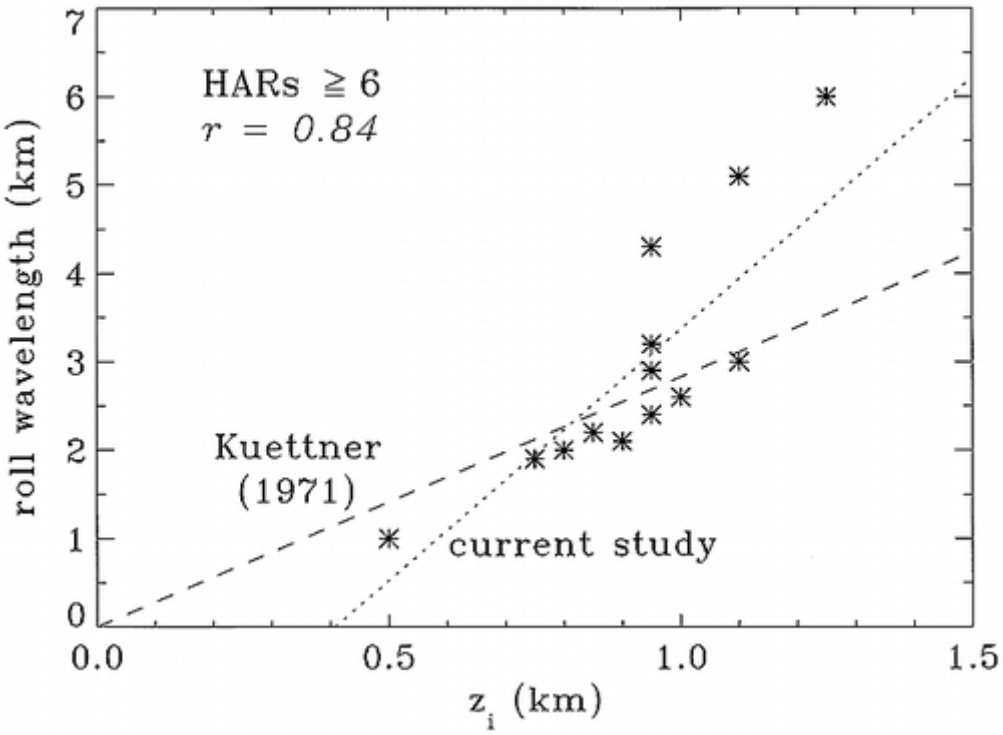

Figure 4.21: Roll wavelength vs. boundary layer depth for various cases from the CaPE experiment. Dashed line indicates theoretical relationship determined by Kuettner (1971). Dotted line is relationship measured by Weckwerth et al. (1997). [From Weckwerth et al. 1997].

Table 4.1 shows the roll wavelength, boundary layer depth, and aspect ratios for several cases from NAME which exhibited the periodic updrafts and downdrafts in the wind profiler data. Roll wavelength was determined from S-Pol reflectivity data, with the wavelength defined as the distance from the center of one roll fine line to the next. Boundary layer depth was determined from 12 UTC soundings, since only 00 UTC and 12 UTC were available on these days. It is possible that the boundary layer depth was greater during the times the periodic vertical motion behavior was observed in the wind profiler data. Aspect ratio was then calculated as described above. As can be seen from Table 4.1, the aspect ratios from HCRs observed during NAME are generally lower than those found in other HCR studies, which would indicate less thermal instability present in the NAME atmosphere. The roll wavelength was determined by measuring the distance

between fine lines observed on S-Pol, which usually showed up around 1500 UTC (well before maximum daytime heating). There would likely be less thermal instability present at this time than later in the day when heating was as its maximum. Therefore, it makes sense that the NAME aspect ratios calculated here are lower than those in previous studies.

Table 4.1: Aspect Ratios for NAME HCR Cases

DATE	ROLL WAVELENGTH [KM]	BOUNDARY LAYER DEPTH [KM]	ASPECT RATIO
31 Jul	2.0	0.7	2.8
2 Aug	1.0	0.5 – 1.0	1.0 – 2.0
7 Aug	1.0	1.0	1.0
8 Aug	1.0	0.8	1.25
10 Aug	1.0	1.0	1.0
11 Aug	1.0	1 – 1.5	1.0 – 1.5

The presence of horizontal convective rolls in the boundary layer when combined with sea breezes might suggest that the two play some role in convective intitiation. Previous studies in Florida, for example, have documented the development of new convection or enhancement of existing convection at HCR and SBF intersection points. In the case of NAME, however, this does not seem to be the case. HCRs, if they are

present in S-Pol PPI images, usually appear and break up into disorganized semi-cellular patterns well before the arrival on land of the sea breeze front.

4.5 Sea Breeze Trigger of Convection

One of the original goals of NAME was to determine the methods that triggered convective development within the core monsoon region. It was initially thought prior to the NAME campaign that the sea breeze played a significant role in triggering convection or possibly organizing and strengthening daily convection that moved down off of the SMO towards the GoC. However, in the analysis of radar data rarely were there cases where the sea breeze initiated any more than a few small pop-up storms. In addition, convection that moved off of the SMO slopes typically arrived on the coastal plain well after the sea breeze front moved onshore and dissipated. If any strengthening of SMO-generated convection did occur due to the sea breeze front's interaction with SMO convection, it was apparently minimal.

The refractivity contrast between the ocean air mass and the land air mass was previously discussed in section 4.3.2. The refractivity values in these two air masses did not appear to differ significantly during NAME. In addition to supporting the idea that the moisture contrast between these two air masses was not significant to cause Bragg scattering at the leading edge of the sea breeze front, it also suggests that the two air masses were not very different in terms of thermal characteristics.

Since thermal contrast is the driving force behind the sea breeze circulation, it can be hypothesized that a weaker thermal contrast between the land and the ocean would lead to weaker sea breezes. From previous analyses, it has been shown that the sea

breeze fine line is often difficult to distinguish in the radar data. One possible explanation for this is that the sea breezes that occurred in NAME were simply much weaker than sea breezes in other locations around the world, in terms of their degree of wind shift. A sea breeze that is weaker would likely not have as much lift along the leading edge, which would diminish its ability to trigger convection.

A lack of thermal contrast in terms of temperature and refractivity could explain why the NAME sea breezes tend to be weaker than in other areas, such as Florida. One factor that differs between the Florida Peninsula and the core NAME region of NW Mexico is the ocean water. In the case of Florida sea breezes, the ocean water on both sides of the peninsula is part of a vast body of water. In NAME, rather than having the entire Pacific Ocean to contrast with the land surface, there is only the Gulf of California. The Gulf of California, when comparing with the Atlantic Ocean or Gulf of Mexico, is much narrower. For the late summer and early fall months of 2004, the surface water temperature in the Gulf of California was higher than that of the water off the coast of Florida. Since cooler ocean water (and warmer land surfaces) is the driving force behind the sea breeze circulation, a warmer ocean surface could certainly explain why the NAME sea breezes aren't as robust as those found in Florida.

Figure 4.22 displays mean sea surface temperature for the NAME region for the months of July 2004 through September 2004. Sea surface temperatures in the Gulf of California, especially near the Eastern coast where S-Pol was located, are upwards of 30° C. The water in this location was much warmer than the SSTs in the open Pacific Ocean at the same latitudes. Sea surface temperatures for Florida for the same time period of July 2004 through September 2004 are shown in Figure 4.23. While water to the

Southwest of the Florida peninsula is around 29°C, water to the East of the peninsula is colder. The contrast in water temperature between these two locations does suggest that the thermal contrast between land and ocean is stronger in Florida than in NW Mexico, at least on the Eastern coast of the GoC. This lack of land-ocean thermal contrast in NW Mexico could help explain why the sea breezes are weaker, in terms of wind shift, in NAME and why this feature does not initiate convection as readily as do sea breezes in Florida. The lack of thermal contrast across the sea breeze front is also consistent with the weak kinematic contrast across the sea breeze front.

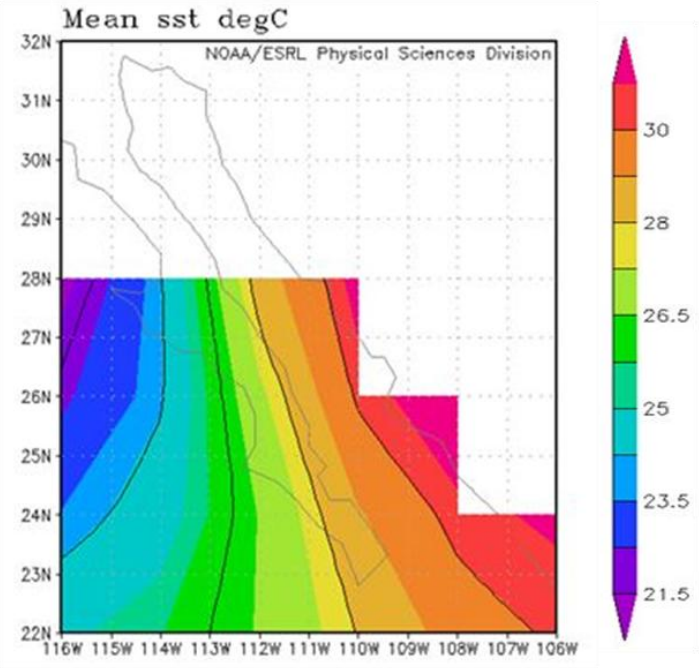

Figure 4.22: 2004 seasonal mean (July through September) sea surface temperature in degrees Celsius for the Gulf of California. [courtesy NOAA]

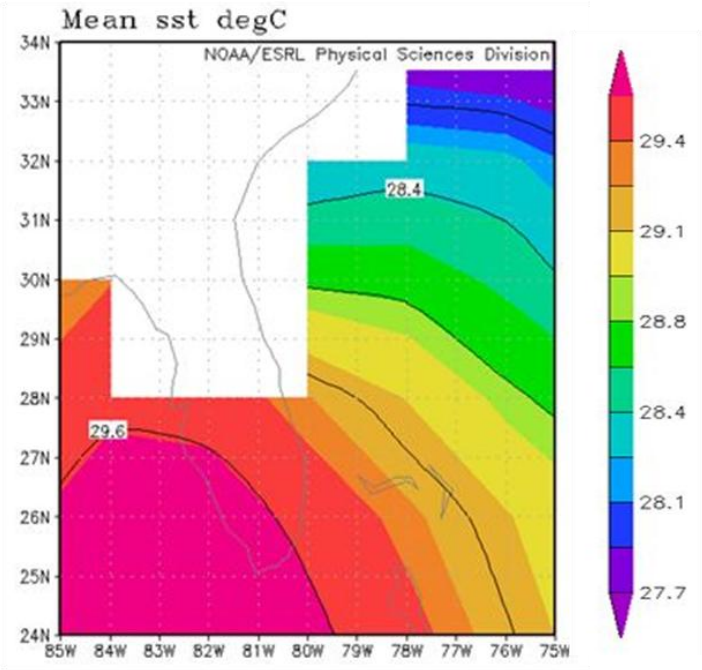

Figure 4.23: As in Figure 4.22, but for the Florida peninsula.

One previous study on Florida sea breezes was conducted by Kingsmill (1995). The thermal contrast between land and ocean air masses for this study was evaluated using soundings, much as was done for the NAME sea breezes. Figure 4.24 shows a figure from Kingsmill (1995). In this example, the DPK station identifier represents the sounding that was released in the warm air mass, ahead of the sea breeze front. The MCL sounding was released in the cool air mass, behind the sea breeze front. In this example, the two soundings are easily distinguished from one another. The temperature in the warm land air mass (DPK) is significantly higher at the surface compared to the temperature in the cool ocean air mass (MCL). In addition, the sounding reveals that the ocean air mass has a higher moisture content than the land air mass up to about 825 mb, as would be expected. Referring back to Figure 4.6, the soundings in the two different air

masses from NAME do not differ as much as the two from the Florida sea breeze study. In fact, the NAME soundings show virtually no moisture difference at the surface, and show the ocean air mass is actually about 1 degree Celsius warmer at the surface than the land air mass. The sounding comparison between the two locations confirms that the thermal contrast in NAME appears to be weaker than that observed in Florida sea breeze studies, and likely explains why the NAME sea breezes are weaker and do not play an important role in initiating convection.

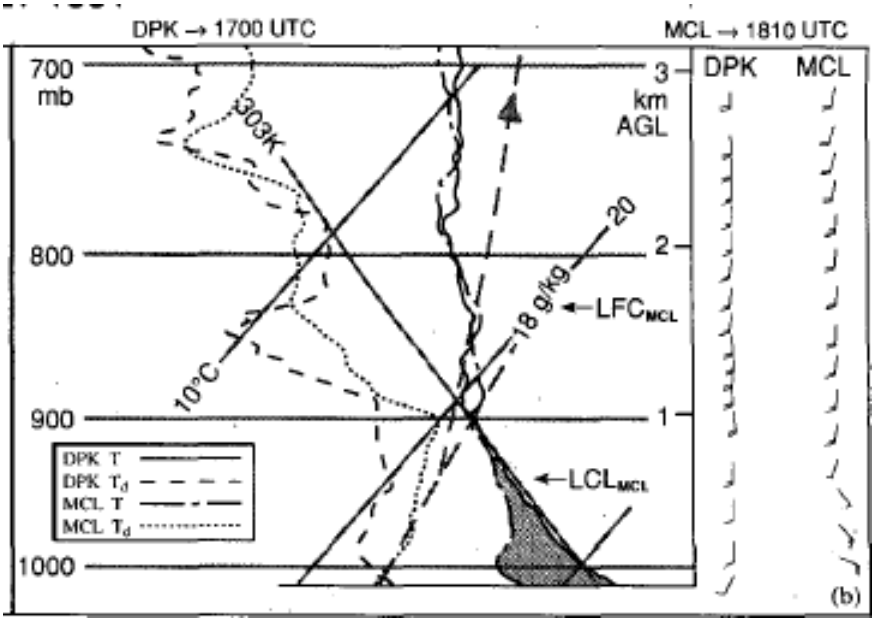

Figure 4.24: Soundings in two air masses from the CaPE experiment in Florida. "DPK" represents the land-based air mass ahead of the sea breeze front. "MCL" denotes the ocean-based air mass behind the SBF. Temperature and dewpoint lines are as indicated in the legend. The shaded area represents the depth of the cool air. Full wind barbs are 5 ms^{-1}. [Adapted from Kingsmill 1995].

CHAPTER 5

Conclusion

5.1 Summary and Conclusions

Use of the NCAR S-Pol radar as well as wind profiler and sounding data has provided a previously unstudied picture of the sea breezes that were observed during NAME. PPI radar analysis proved useful for examining horizontal structure of sea breezes as well as the timing of their arrival and movement on land. Sea breezes typically moved on shore during late morning, or around 1700-1800 UTC. The fine line appeared in the reflectivity field with typical reflectivity values of 10 to 25 dBZ. Sea breezes appeared to dissipate before any significant interactions with SMO based convection could occur over the coastal plain.

It was difficult to examine the vertical structure of the sea breezes using the S-Pol radar data. Background reflectivity features were found to mask the anticipated signature of the sea breeze in the reconstructed RHI plots. However, it was noted that ZDR values throughout the lower atmosphere were quite high, even upwards of 10 dB. It was shown that such high ZDR values could only be explained by oblate scatterers, most likely large insects. High ZDR values were present not only at the leading edge of the sea breeze, but in the boundary layer as a whole which served to obscure the sea breeze signature in the radar data. A further investigation into the scattering mechanisms at work in the sea

breeze fine lines showed that Bragg scattering from variations in the index of refraction was not sufficient to explain reflectivity values of 10 to 25 dBZ from an S-band radar such as S-Pol. Rayleigh scattering from large insects was the most likely mechanism producing the sea breeze fine line echoes in NAME.

Since S-Pol data did not provide as much insight into the vertical structure of sea breezes as was originally hoped, wind profiler data were used. The relative reflectivity and vertical velocity from the profiler occasionally showed updrafts at the time of sea breeze passage as well as a slight enhancement in reflectivity, but the signal was again hard to distinguish from other boundary layer features. However, on some days distinct patterns of repeating updrafts and downdrafts were observed. Comparison with S-Pol PPI data suggested that these were due to the presence of horizontal convective rolls in the NAME boundary layer. While rolls were present on some days, they did not appear to cause an enhancement of existing convection or serve as a mechanism to initiate new convection through interactions with sea breezes. Wind profiler observed horizontal winds revealed that, in some cases, the structure of the leading edge of the sea breeze is consistent with past studies that compare sea breezes to density currents. In these cases, the "head" of the sea breeze front extends more in the vertical compared to the flow that follows.

As to the sea breeze's role in triggering or modulating convection, it appears to be minimal. The sea breeze rarely triggered any significant convection on its own. It was hypothesized that the NAME sea breezes are relatively weak kinematically compared to sea breezes observed in other locales, such as the Florida peninsula. A comparison of seasonal mean sea surface temperatures between the GoC and the water around Florida

reveal that there is a slight temperature difference. The ocean off the coast of Florida, particularly its eastern coast, was cooler than that in the GoC. This implies that the thermal contrast between land and ocean, which is the driving mechanism behind the sea breeze circulation, may be stronger in Florida compared to the the core NAME region. Thus, sea breezes that occur on the Florida peninsula could be stronger (from a kinematic perspective) than those in NAME, perhaps enabling the Florida sea breezes to better initiate convection.

While previous research suggested that the NAME sea breezes played an important role in modulating preexisting convection, such as storms that originate over the SMO and move westward down the slopes toward the coastal plain, this did not seem to be the case. The sea breeze had almost always dissipated by the time any significant SMO convection arrived on the coastal plain. The timing of the SMO convection and the sea breeze front reaching the coastal plain seems to be too far apart for the sea breeze to play any significant role in organizing the NAM convection and resultant precipitation.

REFERENCES

Achtemeier, Gary L., 1991: The Use of Insects as Tracers for "Clear-Air" Boundary-Layer Studies by Doppler Radar. *J. Atmos. Oceanic Technol.*, **8**, 746–765.

Adams, David K., Andrew C. Comrie, 1997: The North American Monsoon. *Bull. Amer. Meteor. Soc.*, **78**, 2197–2213.

Atkins, Nolan T., Roger M. Wakimoto, Tammy M. Weckwerth, 1995: Observations of the Sea-Breeze Front during CaPE. Part II: Dual-Doppler and Aircraft Analysis. *Mon. Wea. Rev.*, **123**, 944–969.

Atkins, Nolan T., Roger M. Wakimoto, 1997: Influence of the Synoptic-Scale Flow on Sea Breezes Observed during CaPE. *Mon. Wea. Rev.*, **125**, 2112–2130.

Atlas, D., W. H. Paulsen, R. J. Donaldson, A. C. Chmela, and V. G. Plank, 1953: *Observations of the sea breeze by 1.25 cm radar.* Proc. Conf. Radio Meteor., Univ. Texas, Paper XI 6.

Atlas, David, 1960: RADAR DETECTION OF THE SEA BREEZE. *J. Meteor.*, **17**, 244–258.

Battan, Louis J. *Radar Meteorology*. Chicago: University of Chicago Press, 1959.

Browning, Keith A., David Atlas, 1966: Velocity Characteristics of Some Clear-Air Dot Angels. *J. Atmos. Sci.*, **23**, 592–604.

Carbone, R. E., J. W. Wilson, T. D. Keenan, J. M. Hacker, 2000: Tropical Island Convection in the Absence of Significant Topography. Part I: Life Cycle of Diurnally Forced Convection. *Mon. Wea. Rev.*, **128**, 3459–3480.

Christian, Thomas W., Roger M. Wakimoto, 1989: The Relationship between Radar Reflectivities and Clouds Associated with Horizontal Roll Convection on 8 August 1982. *Mon. Wea. Rev.*, **117**, 1530–1544.

Ciesielski, Paul E., Richard H. Johnson, 2008: Diurnal Cycle of Surface Flows during 2004 NAME and Comparison to Model Reanalysis. *J. Climate*, **21**, 3890–3913.

Dailey, Peter S., Robert G. Fovell, 1999: Numerical Simulation of the Interaction between the Sea-Breeze Front and Horizontal Convective Rolls. Part I: Offshore Ambient Flow. *Mon. Wea. Rev.*, **127**, 858–878.

Davis, W.M.; L.G. Schultz and R. DE C. Ward. 1890. An investigation of the sea-breeze. *Ann. Harv. Coll. Obs.* Cambridge, Mass. **21**:215-263

Donaldson, R. J., D. Atlas, W. H. Paulsen, R. M. Cummingham, and A. C. Chmela, 1953: *Quantitative 1.25 cm observations of rain and fog.* Proc. Conf. Radio Meteor., Univ. Texas, Paper VII 6.

Donaldson, R. J., 1955: *Drop size distribution, liquid water content, optical transmission, and radar reflectivity in fog and drizzle.* Proc. 5th Wea. Radar Conf., Signal Corps Eng. Lab., Ft. Monmouth, N. J., 275-280.

Douglas, Michael W., 1995: The Summertime Low-Level Jet over the Gulf of California. *Mon. Wea. Rev.*, **123**, 2334–2347.

Douglas, Michael W., Robert A. Maddox, Kenneth Howard, Sergio Reyes, 1993: The Mexican Monsoon. *J. Climate*, **6**, 1665–1677.

Fisher, Edwin L., 1960: AN OBSERVATIONAL STUDY OF THE SEA BREEZE. *J. Meteor.*, **17**, 645–660.

Garand, Louis, Christopher Grassotti, Jacques Hallé, Gerald L. Klein, 1992: On Differences in Radiosonde Humidity-Reporting Practices and Their Implications for Numerical Weather Prediction and Remote Sensing. *Bull. Amer. Meteor. Soc.*, **73**, 1417–1423.

Gray, B. M., 1991: CaPE experiment proceeds in Florida. *Bull. Amer. Meteor. Soc.*, **72**, 1287.

Hajovsky, R. G., and A. H. LaGrone, 1965: The effects of aerosols and insects in the atmosphere on the propagation of microwave signals. Report No. NSF P-1, Antennas & Propagation Division, Electrical Engineering Research Laboratory, The University of Texas, 48 pp.

Higgins, Wayne, and Coauthors, 2006: The NAME 2004 Field Campaign and Modeling Strategy. *Bull. Amer. Meteor. Soc.*, **87**, 79–94.

Keenan, T., and Coauthors, 2000: The Maritime Continent Thunderstorm Experiment (MCTEX): Overview and Some Results. *Bull. Amer. Meteor. Soc.*, **81**, 2433–2455.

Kingsmill, David E., 1995: Convection Initiation Associated with a Sea-Breeze Front, a Gust Front, and Their Collision. *Mon. Wea. Rev.*, **123**, 2913–2933.

Kuettner, J. P., 1971: Cloud bands in the earth's atmosphere. *Tellus,* **23,** 404-425.

Lang, Timothy J., Steven A. Rutledge, Jeffrey L. Stith, 2004: Observations of Quasi-Symmetric Echo Patterns in Clear Air with the CSU–CHILL Polarimetric Radar. *J. Atmos. Oceanic Technol.*, **21**, 1182–1189.

Lang, Timothy J., David A. Ahijevych, Stephen W. Nesbitt, Richard E. Carbone, Steven A. Rutledge, Robert Cifelli, 2007: Radar-Observed Characteristics of Precipitating Systems during NAME 2004. *J. Climate*, **20**, 1713–1733.

Lang, Timothy J., Steven A. Rutledge, Robert Cifelli, 2010: Polarimetric Radar Observations of Convection in Northwestern Mexico during the North American Monsoon Experiment. *J. Hydrometeor*, **11**, 1345–1357.

LeMone, Margaret Anne, 1973: The Structure and Dynamics of Horizontal Roll Vortices in the Planetary Boundary Layer. *J. Atmos. Sci.*, **30**, 1077–1091.

Mueller, Eugene A., Ronald P. Larkin, 1985: Insects Observed Using Dual-Polarization Radar. *J. Atmos. Oceanic Technol.*, **2**, 49–54.

Nicholls, Melville E., Roger A. Pielke, William R. Cotton, 1991: A Two-Dimensional Numerical Investigation of the interaction between Sea Breezes and Deep Convection over the Florida Peninsula. *Mon. Wea. Rev.*, **119**, 298–323.

Pereiera, Luis Gustavo P. "Characteristics and Organization of Precipitating Features During NAME 2004 and their Relationship to Environmental Conditions." PhD Dissertation. Colorado State University, 2008.

Martin Ralph, F., 1995: Using Radar-Measured Radial Vertical Velocities to Distinguish Precipitation Scattering from Clear-Air Scattering. *J. Atmos. Oceanic Technol.*, **12**, 257–267.

Rowe, Angela K., Steven A. Rutledge, Timothy J. Lang, Paul E. Ciesielski, Stephen M. Saleeby, 2008: Elevation-Dependent Trends in Precipitation Observed during NAME. *Mon. Wea. Rev.*, **136**, 4962–4979.

Rowe, Angela K., Steven A. Rutledge, Timothy J. Lang, 2011: Investigation of microphysical processes occurring in isolated convection during NAME. *Mon. Wea. Rev.*, submitted.

Russell, R. W., and J. W. Wilson, 1996: Aerial plankton detected by radar. *Nature,* **381,** 200-201.

Schmidt, F. H., 1947: An elementary theory of the land and sea breeze. *J. Meteor.*, **4**, 9-15.

Sha, Weiming, Takeshi Kawamura, Hiromasa Ueda, 1991: A Numerical Study on Sea/Land Breezes as a Gravity Current: Kelvin–Helmholtz Billows and Inland Penetration of the Sea-Breeze Front. *J. Atmos. Sci.*, **48**, 1649–1665.

Simpson, J. E., 1969: A comparison between laboratory and atmospheric density currents. *Quart. J. Roy. Meteor. Soc.,* **95,** 758-765.

Simpson, J.E., D. A. Mansfield, and J. R. Milford, 1977: Inland penetration of sea-breeze fronts. *Quart. J. Roy. Meteor. Soc.*, **103,** 47-76.

Simpson, J. E., and R. E. Britter, 1980: A laboratory model of an atmospheric mesofront. *Quart. J. Roy. Meteor. Soc.*, **106,** 485-500.

Simpson, Joanne, Gary Van Helvoirt, Michael McCumber, 1982: Three-Dimensional Simulations of Cumulus Congestus Clouds on GATE Day 261. *J. Atmos. Sci.*, **39**, 126–145.

Wakimoto, Roger M., Nolan T. Atkins, 1994: Observations of the Sea-Breeze Front during CaPE. Part I: Single-Doppler, Satellite, and Cloud Photogrammetry Analysis. *Mon. Wea. Rev.*, **122**, 1092–1114.

Weckwerth, Tammy M., Thomas W. Horst, James W. Wilson, 1999: An Observational Study of the Evolution of Horizontal Convective Rolls. *Mon. Wea. Rev.*, **127**, 2160–2179.

Weckwerth, Tammy M., James W. Wilson, Roger M. Wakimoto, N. Andrew Crook, 1997: Horizontal Convective Rolls: Determining the Environmental Conditions Supporting their Existence and Characteristics. *Mon. Wea. Rev.*, **125**, 505–526.

Williams, Christopher R., Allen B. White, Kenneth S. Gage, F. Martin Ralph, 2007: Vertical Structure of Precipitation and Related Microphysics Observed by NOAA Profilers and TRMM during NAME 2004. *J. Climate*, **20**, 1693–1712.

Wilson, James W., Tammy M. Weckwerth, J. Vivekanandan, Roger M. Wakimoto, Robert W. Russell, 1994: Boundary Layer Clear-Air Radar Echoes: Origin of Echoes and Accuracy of Derived Winds. *J. Atmos. Oceanic Technol.*, **11**, 1184–1206.

Zrnić, D. S., and A. V. Ryzhkov, 1998: Observations of Insects and Birds with a Polarimetric Radar. *IEEE Transactions on Geoscience and Remote Sensing,* **32,** 661-668.

Zuidema, Paquita, Chris Fairall, Leslie M. Hartten, Jeffrey E. Hare, Daniel Wolfe, 2007: On Air–Sea Interaction at the Mouth of the Gulf of California. *J. Climate,* **20**, 1649–1661.